



OPEN ACCESS

EDITED BY

Segaran P. Pillai,
United States Department of Health and
Human Services, United States

REVIEWED BY

Thomas Huber,
The Rockefeller University,
United States
Samantha Kasloff,
National Microbiology Laboratory,
Canada

*CORRESPONDENCE

Tony L. Buhr,
tony.l.buhr.civ@us.navy.mil

SPECIALTY SECTION

This article was submitted to Biosafety
and Biosecurity,
a section of the journal
Frontiers in Bioengineering and
Biotechnology

RECEIVED 14 February 2022

ACCEPTED 14 September 2022

PUBLISHED 04 October 2022

CITATION

Buhr TL, Borgers-Klonkowski E,
Gutting BW, Hammer EE, Hamilton SM,
Huhman BM, Jackson SL, Kennihan NL,
Lilly SD, Little JD, Luck BB,
Matuczinski EA, Miller CT, Sides RE,
Yates VL and Young AA (2022),
Ultraviolet dosage and decontamination
efficacy were widely variable across
14 UV devices after testing a dried
enveloped ribonucleic acid virus
surrogate for SARS-CoV-2.
Front. Bioeng. Biotechnol. 10:875817.
doi: 10.3389/fbioe.2022.875817

COPYRIGHT

© 2022 Buhr, Borgers-Klonkowski,
Gutting, Hammer, Hamilton, Huhman,
Jackson, Kennihan, Lilly, Little, Luck,
Matuczinski, Miller, Sides, Yates and
Young. This is an open-access article
distributed under the terms of the
[Creative Commons Attribution License
\(CC BY\)](https://creativecommons.org/licenses/by/4.0/). The use, distribution or
reproduction in other forums is
permitted, provided the original
author(s) and the copyright owner(s) are
credited and that the original
publication in this journal is cited, in
accordance with accepted academic
practice. No use, distribution or
reproduction is permitted which does
not comply with these terms.

Ultraviolet dosage and decontamination efficacy were widely variable across 14 UV devices after testing a dried enveloped ribonucleic acid virus surrogate for SARS-CoV-2

Tony L. Buhr^{1*}, Erica Borgers-Klonkowski¹,
Bradford W. Gutting¹, Emlyn E. Hammer¹, Shelia M. Hamilton¹,
Brett M. Huhman², Stuart L. Jackson², Neil L. Kennihan¹,
Samuel D. Lilly¹, John D. Little Jr², Brooke B. Luck¹,
Emily A. Matuczinski¹, Charles T. Miller¹, Rachel E. Sides¹,
Vanessa L. Yates¹ and Alice A. Young¹

¹Naval Surface Warfare Center-Dahlgren Division, Concepts and Experimentation Branch (B64), Dahlgren, VA, United States, ²Naval Research Laboratory (Plasma Physics Division), Washington, DC, United States

Aims: The dosages and efficacy of 14 ultraviolet (UV) decontamination technologies were measured against a SARS-CoV-2 surrogate virus that was dried onto different materials for laboratory and field testing.

Methods and results: A live enveloped, ribonucleic acid (RNA) virus surrogate for SARS-CoV-2 was dried on stainless steel 304 (SS304), Navy Top Coat-painted SS304 (NTC), cardboard, polyurethane, polymethyl methacrylate (PMMA), and acrylonitrile butadiene styrene (ABS) materials at > 8.0 log₁₀ plaque-forming units (PFU) per test coupon. The coupons were then exposed to UV radiation during both laboratory and field testing. Commercial and prototype UV-emitting devices were measured for efficacy: four handheld devices, three room/surface-disinfecting machines, five air disinfection devices, and two larger custom-made machines. UV device dosages ranged from 0.01 to 729 mJ cm⁻². The antiviral efficacy among the different UV devices ranged from no decontamination up to nearly achieving sterilization. Importantly, cardboard required far greater dosage than SS304.

Conclusion: Enormous variability in dosage and efficacy was measured among the different UV devices. Porous materials limit the utility of UV decontamination.

Significance and impact of the study: UV devices have wide variability in dosages, efficacy, hazards, and UV output over time, indicating that each UV device needs independent technical measurement and assessment for product development prior to and during use.

KEYWORDS

UV decontamination, enveloped virus $\Phi 6$, enveloped virus, decontamination, ultraviolet (UV), SARS-CoV-2, COVID-19

Introduction

Tremendous attention was directed at the subject of UV decontamination during the COVID-19 pandemic, even though UV devices are best used to augment other sanitation techniques rather than for stand-alone decontamination (Raiszadeh and Adeli 2020; Memarzadeh 2021). Numerous devices that incorporate UV sources including handheld devices, room decontamination devices, and water treatment devices are available on the market to decontaminate air, water, and surface materials. Variability in UV devices is extensive and includes differences in electronics, UV sources, power, and product designs. The distance from UV sources at which decontamination/inactivation occurs is also widely variable, ranging from a couple of centimeters to a couple of meters. UV sources also differ and include mercury (Hg), krypton chloride (KrCl), xenon (Xe), and various light emitting diodes (LEDs), which range in wavelength, and there are several different manufacturers. In addition, although Hg bulbs are the most common, Hg bulb dosage significantly varies over time after the Hg bulb is turned on. Hg also comes with the risk of toxicity, although that risk is similar to fluorescent light bulbs. The variability in these decontamination devices is further complicated by variability in test methods, which include different virus preparation methods, tests with unpurified vs. purified virus, tests with wet virus or dried virus, the presence of organic debris, and differences in the porosity of surface materials. Assessments of UV for decontamination must also take into account maintenance since UV sources need to be cleaned in order to maintain dosage (United States Food and Drug Administration 2021a; United States Environmental Protection Agency 2021).

UV radiation, particularly UV-C, is a known microbe disinfectant for air, water, and non-porous surfaces (United States Food and Drug Administration 2021a; United States Environmental Protection Agency 2021). UV-C primarily inactivates microbes including viruses if they are directly exposed to the UV radiation. Therefore, inactivation is far less effective if a microbe is associated with soil, dust, oils, and any type of host cell debris or if it is embedded in porous materials (United States Food and Drug Administration 2021a). This is particularly relevant for obligate pathogens such as viruses, which are naturally associated with host cell components and body fluids: mucus in the case of respiratory virus such as SARS-CoV-2 (Aps and Martens, 2005; Heimbuch et al., 2011; Vejerano and Marr 2018). The effectiveness of UV-C lamps in inactivating environmentally relevant SARS-CoV-2 virus is unknown because there are limited consistent and/or reliable published data about the wavelength, dose, and

duration of UV-C radiation required to inactivate the SARS-CoV-2 virus, particularly in its natural (unpurified) state (United States Food and Drug Administration 2021a; United States Environmental Protection Agency 2021). This is true of all viruses because UV efficacy is further complicated by the fact that methods for virus preparation and testing, particularly enveloped viruses, are highly variable among laboratories (Hadi et al., 2020). Purified enveloped viruses are often tested in laboratories, even though these viruses only exist naturally when associated with host cell components and debris in nature, and they can be compromised during purification (Cox and Wathes 1995).

The stability of viral particles in the environment depends on temperature and humidity, as well as characteristics of the virus itself as it is shed from the host (Cox and Wathes 1995). Human respiratory droplets are mainly composed of mucus (salt, mucin glycoprotein, and lipids (surfactants)), and these components can shield the virus from UV and affect decontamination kinetics (Vejerano and Marr 2018; Hadi et al., 2020). The mean size of infectious, respirable particles is 4 μm for a 50% probability of a thoracic deep lung deposition (Brown et al., 2013). Particles $>10 \mu\text{m}$ do not go past the larynx, and particles $<1 \mu\text{m}$ have lower probabilities of deposition (Brown et al., 2013; Hofer et al., 2021). Measurements of SARS-CoV-2 respiratory droplets are typically 0–1 virions per speech particle, and the water in SARS-CoV-2 respiratory particles evaporates within seconds to generate dry particles around 4 μm , right at the respirable size range (Stadnytskyi et al., 2020). Hence, the virus respiratory size is much larger than the size of a naked coronavirus, which is 78 nm for SARS-CoV-2 (Goldsmith et al., 2004) and can range from 50 to 200 nm (Masters 2006). A volume/volume calculation with a 78 nm virus and 4 μm particle equates to $>99.999\%$ mucus and $<0.001\%$ virus per particle and sets a minimum target on the ratio of debris to virus expected for decontamination testing. This only accounts for debris in respiratory particles and does not account for additional debris that might be found on surfaces. In addition, enveloped viruses are more stable under dry conditions than wet environments (Cox and Wathes 1995; Chan et al., 2011; van Doremalen et al., 2013; Buhr et al., 2020; Hadi et al., 2020), and drying viruses *via* lyophilization is frequently used to stabilize virus for long-term storage (Greiff et al., 1954; Greiff and Richtel 1966; Malenovska 2014). Hence, decontamination kinetics can also be greatly influenced depending on whether the test microbes are wet or dry. Rhinotillexis (nose-picking) creates additional environmental loads of infectious virus, which is also composed of mucus mixed with unpurified virus and varying levels of free water (Hendley et al., 1973; Weber and Stilianakis, 2008).

In addition to method gaps to define, characterize, and standardize SARS-CoV-2 virus debris composition and drying, standardized methods for reproducibly preparing high titers ($>10 \log_{10}$ of virus ml^{-1} of culture medium at the time of virus harvest) of SARS-CoV-2 for testing without artificial post-harvest cleaning and concentration steps are needed for statistical confidence and to match virus levels in the environment. Furthermore, there were/are urgent needs during the COVID-19 pandemic to test decontamination devices, like UV, in field tests outside of laboratory containment. Viruses that fall under the higher World Health Organization (WHO) biosafety level (BSL) classifications such as SARS-CoV-2 (BSL-3) and its BSL-2 surrogate coronaviruses (ASTM International 2020) cannot be widely used in field tests because of cost, time, and safety constraints. For field testing, the enveloped virus surrogate $\Phi 6$ was previously used to make “live/dead” $\Phi 6$ test indicators to directly test and compare decontamination efficacy across laboratory and field tests (Buhr et al., 2020).

Surrogates are often used as models in studies of decontamination for highly infectious pathogens. Bacteriophages are useful for this purpose as they are similar in terms of morphology, behavior in the environment, and surface properties, but BSL-1 are easier to isolate at high titers ($>10 \log_{10} \text{ml}^{-1}$ without virus purification and concentration) for testing than mammalian viruses (Gallandat and Lantagne, 2017). Among bacteriophages, $\Phi 6$ has been identified as a preferred surrogate for enveloped viruses including influenza and SARS-CoV-2 (Bibby et al., 2015; Gallandat and Lantagne 2017; Vejerano and Marr 2018; Buhr et al., 2020; Fedorenko et al., 2020). *Pseudomonas* virus $\Phi 6$ is a BSL-1 enveloped RNA virus originally isolated in a bean field as a lytic virus that infects the plant pathogenic bacterium *Pseudomonas syringae* pathovar *phaseolicola* (Vidaver et al., 1973; Van Etten et al., 1976; Mindich 2004). The $\Phi 6$ envelope structure is similar to many other enveloped viruses as the envelope consists of a glycoprotein/protein-embedded lipid membrane, and the host cell has similar temperature sensitivity to mammalian cells at around 40°C . This is important since the envelope components are considered a target for inactivation by many different decontaminants including UV radiation, particularly at 222 nm (McDonnell and Burke, 2011; Wiggington et al., 2012; Hadi et al., 2020; United States Food and Drug Administration 2021a). $\Phi 6$ is a 13.5 kb double-stranded RNA (dsRNA) phage (Mindich, 2004), and spherical (80–100 nm diameter) with structural similarity to coronaviruses (50–200 nm diameter). The 13.5 kb dsRNA genome, the equivalent of 27 kb of single-stranded RNA (ssRNA), is comparable to the 26–32 kb of ssRNA in coronaviruses. In theory, a surrogate virus should have a similar number of adjacent pyrimidines compared to SARS-CoV-2 since pyrimidine dimerization is considered an important mechanism of UV inactivation (Heßling et al., 2020). Based on pyrimidine target numbers only, $\Phi 6$ (6,613 adjacent pyrimidine pairs) and SARS-CoV-2 (7,600 pairs) should have similar UV sensitivity, although ssRNA may be slightly more sensitive than dsRNA due to the potential for repair of dsRNA by the undamaged

strand (Tseng and Li, 2005). Hence, sequence data alone theoretically imply that $\Phi 6$ inactivation goals should be similar to or slightly more conservative than SARS-CoV-2. Separately, it is currently difficult to compare UV efficacy both within and across different viruses based on existing data because experimental tests are highly variable across different laboratories and studies (Hadi et al., 2020). Overall, the sequence comparison between the two viruses is likely moot because debris, drying, and porosity of respiratory particles and/or contaminated surfaces have dominant impacts on decontamination kinetics, particularly when the amount of debris is $>99.999\%$ relative to virus (United States Food and Drug Administration 2021a; United States Environmental Protection Agency 2021). Furthermore, practical confidence that test methods approach the challenge of field conditions is needed from field decontamination testing in order to increase confidence in devices to be employed by end users (Hamilton et al., 2013; Buhr et al., 2015, 2016).

Here, $\Phi 6$ was prepared at $11.0 \pm 0.2 \log_{10}$ PFU ml^{-1} without post-harvest processing or concentration steps, and then dried on to different materials for >24 h (h) to make BSL-1 live/dead enveloped virus test indicators at $\geq 8.0 \log_{10}$ PFU coupon $^{-1}$. Numerous UV devices were tested in both laboratory and field trials for both screening and iterative UV product improvement. As a BSL-1 surrogate, $\Phi 6$ is useful for the generation of baseline decontamination data for enveloped viruses, particularly during the COVID-19 pandemic when results from field decontamination methods and procedures were urgently needed. It is recognized that the limitation of $\Phi 6$ testing is that a correlation test with ≥ 5 independent batches of unpurified mammalian coronavirus at $\geq 8.0 \log_{10}$ PFU coupon $^{-1}$ is needed. The current limitation of such a correlation test is linked to limitations with coronavirus preparation and test methods. COVID-19 mucus is significantly thicker than healthy mucus (Kratovich et al., 2022), but not yet defined for virus inactivation testing. This natural microbial protectant will need to be standardized and combined with virus to generate practical confidence for SARS-CoV-2 inactivation data. In addition, titers of laboratory-prepared coronavirus need to be significantly higher in order to meet the virus load that has been measured and is expected in the environment. Thus, while there are limitations to this study, the $\Phi 6$ test met the quantitative, practical objectives, and was the most conservative live/dead enveloped virus test known for field testing during COVID-19 and for screening/selecting decontamination equipment and technologies (Buhr et al., 2020).

Materials and methods

$\Phi 6$ and host cell preparations

Virus and host cell preparation was previously described (Buhr et al., 2020). $\Phi 6$ and its host organism *P. syringae* pathovar

phaseolicola HB10Y (HB10Y), causal agent of halo blight of the common bean, *Phaseolus vulgaris*, were isolated in Spain. Both were a kind gift from Dr. Leonard Mindich at Rutgers University, New Jersey Medical School. HB10Y was prepared by inoculating 100–200 ml of 3% tryptic soy broth (TSB; Fluka PN#T8907-1KG) in a 1-L (L) smooth-bottom Erlenmeyer flask with a high efficiency particulate air (HEPA) filter cap. Cultures were incubated at $26 \pm 2^\circ\text{C}$, 200 revolutions (rev) minute (min)⁻¹ for 20 ± 2 h. 11.1 ml of 100% glycerol (Sigma PN #G7757-500 ML) was added per 100 ml of host culture. Final concentration of glycerol was 10%; 1-ml aliquots of HB10Y were pipetted into screw-cap microfuge tubes with O-rings and stored at -80°C . HB10Y samples were titered prior to freezing by serially diluting samples in 10 mM (mM) of 4-(2-hydroxyethyl)-1-piperazineethanesulfonic acid (HEPES, Sigma PN#H4034-100G) + 10% sucrose (Sigma PN #S7903-250G), pH 7.0, and plating on tryptic soy agar (TSA; Hardy Diagnostics, Santa Maria, CA). The plates were inverted and incubated at $26 \pm 2^\circ\text{C}$ for 48 ± 2 h to show titers of $\sim 10^9$ cells ml⁻¹. After freezing, tubes were thawed at room temperature (RT, $22 \pm 3^\circ\text{C}$), serially diluted, and plated to show sustained viability after long-term storage at -80°C .

$\Phi 6$ was prepared after inoculating broth cultures of HB10Y. A frozen stock preparation of HB10Y was thawed at $22 \pm 3^\circ\text{C}$. HB10Y was added either directly from a frozen stock or by transferring a single colony from a streaked TSA plate to 200 ml of 3% TSB in a 1-L smooth-bottom Erlenmeyer flask with a HEPA cap and incubated at $26 \pm 2^\circ\text{C}$, 200 rev min⁻¹ overnight. The cells were then diluted and grown to mid-log phase ($3\text{--}5 \times 10^8$ cells ml⁻¹). The host flask was inoculated with 0.5–1 ml of $\Phi 6$ at a stock concentration of $11 \pm 0.2 \log_{10}$ PFU ml⁻¹. The culture was incubated at $26 \pm 2^\circ\text{C}$, 200 rev min⁻¹ for 24 ± 2 h. The $\Phi 6$ preparation was stored at 4°C until titering was completed. After titer determination was completed, 1–1.3 ml volumes were aliquoted into 1.5-ml screw-cap tubes with O-rings, inverted, and stored at -80°C .

Coupon materials and sterilization

2 cm (cm) x 2 cm coupons of different test materials were inoculated with $\geq 8.0 \log_{10}$ PFU $\Phi 6$ virus inoculum (Buhr et al., 2020). Materials for inoculation included stainless steel 304 (SS304) (20-gauge with a 2B finish from Cardinal Scientific), SS304 coupons painted with Navy Top Coat (NTC) (26-gauge SS304 with a 2B finish primed with N-6237 and top coated with MIL-PRF-24635B, 4–6 mils from the Coatings Group at the University of Dayton Research Institute (Dayton, OH, United States)), acrylonitrile butadiene styrene (ABS) plastic (flat black coupon from Cardinal Scientific), polymethyl methacrylate (PMMA) plastic (keyboard keys from Hewlett-Packard computer keyboards), polyurethane (clear polyurethane national stock number 9330-01-541-8524X3),

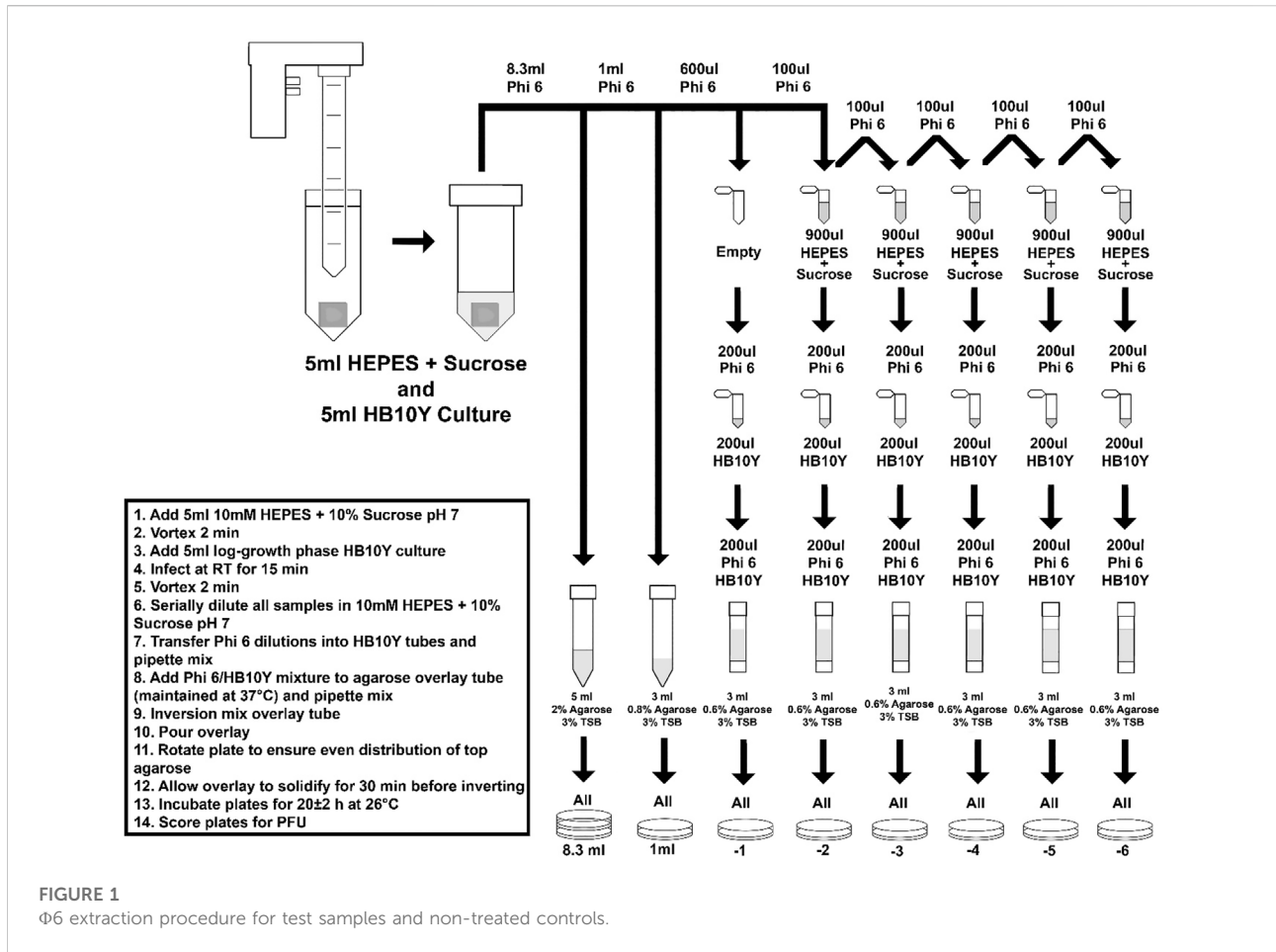
and cardboard (hand-cut from Corrugated Recycles, new, single wall, cardboard box (Davis Core & PAD, Cave Spring, Ga, United States) with thickness of 0.16 inch). ABS and PMMA plastics are often used for computer keyboards. The plastics and SS304 represent non-porous materials. NTC represents semi-porous surfaces found on military ships. Cardboard represents porous materials used in shipping although it is not as porous as fabrics or carpeting.

For sterilization, SS304 and NTC coupons were rinsed with 18 mega-ohm-cm, de-ionized water, placed on an absorbent paper in an autoclave-safe container, and autoclaved for 30 min at 121°C , 100 kPa. PMMA keyboard keys were removed, trimmed, cleaned with soap, then rinsed with de-ionized water, and wrapped in aluminum foil. ABS coupons were similarly rinsed with de-ionized water and wrapped in foil. Cardboard coupons were devoid of noticeable debris, flaws, and ink and were wrapped in foil. After wrapping in foil, the PMMA keyboard keys, ABS, and cardboard were all sterilized *via* hot, humid air at 95°C and 90% relative humidity (RH) for 4 h. Polyurethane coupons, having been pre-cut, were soaked in ethanol to remove ink residue left over from the cutting process. They were then rinsed with de-ionized water, sterilized *via* immersion in 70% ethanol for more than 20 min, and allowed to dry. All sterilized coupons were stored in sterile containers until used.

Coupon inoculation, extraction, and quantitation

Five independent preparations of $\Phi 6$ were removed from -80°C storage and thawed at $22 \pm 3^\circ\text{C}$. Working inoculum was prepared by transferring stock $\Phi 6$ into 50-ml conical tubes containing 10 mM HEPES +10% sucrose pH 7.0, with a final concentration of $\sim 9 \log_{10}$ PFU ml⁻¹. Coupons were inoculated with 0.1 ml of $\Phi 6$ working inoculum and subsequently held at $22 \pm 3^\circ\text{C}$ for more than 24 h to dry and adhere to the material. The PMMA keyboard keys were slightly slanted. Therefore, during inoculation and drying, the keys were positioned on a sterilized surface, which was elevated on an incline *via* slats to provide a level inoculation surface.

Once the inoculum had dried onto the coupons, they were exposed to UV from the candidate devices. Specific parameters for testing the individual devices varied but coupon number and preparation prior to testing was maintained across all experiments. For each test, five individual coupons were included for each of the test materials (SS304, cardboard, NTC, polyurethane, and either PMMA plastic keyboard keys or ABS plastic). Each coupon was inoculated with one of five independent virus preparations as described earlier. Extraction and shipping control coupons (inoculated and transported to the testing sites but not exposed to UV radiation) and negative control coupons that are not inoculated with virus were also



included for every experiment. Finally, the $\Phi 6$ virus inoculum used to prepare the coupons was maintained at RT from the date of coupon inoculation through the test, and viral titer was measured at the conclusion of test exposures for each experiment.

To increase confidence in decontamination results and to conservatively estimate decontamination requirements for enveloped virus in its native state, enveloped virus test coupons were prepared to be protected similar to a natural virus without interfering with the virus assay. Thus, $\Phi 6$ virus was unpurified to maintain natural stabilization with host cell debris and was diluted in a 10% sucrose solution to mimic the presence of carbohydrates in mucus without inhibiting the decontamination assay (Brakke, 1951; Malenovska, 2014; Buhr et al., 2020; Hadi et al., 2020; Stadnytskyi et al., 2020). In addition, enveloped virus was dried on coupons prior to testing since SARS-CoV-2 respiratory particles evaporate within seconds to generate dry particles, and drying on fomites is also historically documented as a route of infection for enveloped virus (Fenn, 2001; Malenovska, 2014; Hadi et al., 2020; Stadnytskyi et al., 2020).

After UV exposure, virus was extracted from both test and control coupons (Figure 1) and plated in <25 min using a $\Phi 6$ extraction and overlay procedure that was previously described (Buhr et al., 2020). For $\Phi 6$ extraction from materials (coupons), 5 ml of 10 mM HEPES +10% sucrose pH 7 were added to each conical tube with a virus-inoculated coupon and vortexed for 2 min. After vortexing, 5 ml of HB10Y log-phase culture (confirmed with real-time Coulter Multisizer analysis) were added and allowed to infect at RT for 15 min, followed by 2 min of vortexing. Each sample was serially diluted, from -2 to -6, in 900 μ L of 10 mM HEPES +10% sucrose pH 7. For each $\Phi 6$ dilution, from -1 to -6, 200 μ L was transferred into individual tubes containing 200 μ L log-phase HB10Y. Then, 200 μ L of those $\Phi 6$ /HB10Y mixtures were added to individual TSB overlay tubes, poured onto individual TSA plates, and allowed to solidify for ≥ 30 min. In addition, 1,000 μ L was transferred from the 50 ml sample conical tube directly to a TSB overlay tube, and the remaining 8.3 ml was poured onto two TSA plates and also allowed to solidify for ≥ 30 min. Solidified plates were then inverted, incubated for 20 \pm 2 h at 26°C, and

quantified. The plates were incubated for an additional 24 h, RT and quantified a final time.

Quantitation and calculations of survival were performed as previously described (Buhr et al., 2020). An important difference between virus and prior spore quantitation is that virus and spore inoculum dried on to coupons were stable. However, titers of virus controls stored in solution were unstable and highly variable, whereas spore controls were stable in solution. Therefore, virus inoculation titers were defined as 100% extraction, or maximum recoverable virus, and used to calculate the extraction efficiency for each material.

Virus survival and \log_{10} reduction were then quantified using ASTM standard practices E3092 and E3178 except plaque-forming units (PFU) replaced colony-forming units (CFU) (ASTM International, 2018a; ASTM International, 2018b; Buhr et al., 2014). The sample mean and sample standard deviations were calculated for each set of samples. The virus inoculation titer adjusted for the volume and dilution difference served as the 100% recovery reference value for calculating the virus survival after decontamination. The extraction percentage was an arithmetic calculation and not a \log_{10} calculation. The extraction percentage was calculated by dividing the total number of infectious virus (PFU) extracted from the virus-inoculated control coupons for each material type by the total number of inoculated virus (PFU) (divided by 100 to adjust for 0.1 ml of viral inoculum deposited on each coupon and the 10 ml extraction volume). The average extraction efficiency was calculated and recorded for each type of test material for each test day. The number of surviving PFU for each test coupon was corrected for extraction efficiency by dividing the number of surviving PFU by the extraction percentage to determine the total number of PFU ml^{-1} . The virus survival of each test coupon (corrected for extraction efficiency) in PFU ml^{-1} was multiplied by 10 to account for the 10 ml total volume in each tube with extraction buffer. This gave the total number of surviving PFU per sample. The virus survival of each control coupon in PFU ml^{-1} was also multiplied by 10 to account for the 10 ml of extraction volume. Each number was converted to \log_{10} . Since the \log_{10} of 0 is infinite, the number '1' was added for simplicity to each number prior to converting to \log_{10} . The \log_{10} mean and \log_{10} standard deviation was calculated for infectious virus for each coupon material. The \log_{10} reduction mean and standard deviation were calculated for each coupon material. For \log_{10} reduction, the \log_{10} mean of each coupon material was subtracted from the \log_{10} mean of the virus titer (minus 1 to adjust for 0.1 ml of viral inoculum deposited on to each coupon), the 100% recovery reference value. For the \log_{10} reduction standard deviation, the square root of the result of the \log_{10} survival standard deviation was taken for each coupon squared; divided by the number of independent samples plus the \log_{10} survival standard deviation of the virus inoculum titer squared; and divided by the number of independent samples.

Spectroscopic analysis hardware and calibration

The primary spectrometer used for this work was the Ocean Optics Maya 2000 Pro, which measured optical spectra from 180–630 nm with an average bin size of 0.22 nm across the measurable spectrum. The distribution is not strictly linear, but can be specifically determined as necessary for data processing. The spectrometer was used with a fiber bundle (BFL200HS02), which incorporates seven $\Phi 200\text{-}\mu\text{m}$ core fibers into a single high-OH package. This enables the measurement of sources with low output so the spectrometer can both retain a high signal-to-noise ratio and enable the use of a cosine corrector (CCSA2) for most measurements.

The Maya 2000 Pro spectrometer was calibrated using a Cathodeon R48 Deuterium Lamp, serial number CH5627. The spectral irradiance from this lamp is in units of $\text{mW}\cdot\text{m}^{-2}\cdot\text{nm}^{-1}$ in 5 nm intervals from 200 to 400 nm. To perform the calibration, the lamp is mounted vertically and positioned so that a horizontal line through the center of the area to be irradiated passes through the center of the lamp emission area, as well as perpendicular to the lamp window. The calibration refers to the spectral irradiance over an approximately 10 mm^2 area in a vertical plane located at a distance of 200 mm from the outside surface of the output window on the lamp. The lamp is operated from a 300-mA power supply and must be operated continuously for 30 min prior to recording data on the spectrometer.

The spectrometer was mounted on an optical table, with a three-axis linear translation stage (Thorlabs LTS300) used to enable precision alignment between the spectrometer fiber sensor head and the source of interest. The three-axis system is capable of measuring a 300 mm \times 300 mm \times 300 mm volume with computer automation using a process-controlled script *via* Thorlabs Kinesis software. The data acquisition software used National Instruments LabVIEW for all aspects except direct control of the translation stages. All of the data were written to a single Technical Data Management Streaming data file for post-processing, which enabled all of the measurements to have a common time base for analysis. Post-processing was accomplished with the Jupyter software environment with discrete Python code blocks to allow for processing of specific sources as needed. The raw TDMS data file is loaded into a cache file on the processing server, and a series of factors and calibrations are applied to prepare the raw data for analysis. Static measurements are relatively simple, as the position is fixed and no further analysis is required. Sweeps in a two-dimensional space with the translation stages requires synchronization of the position with digital fiducial markers to construct an image of the measured plane at a given distance from the source.

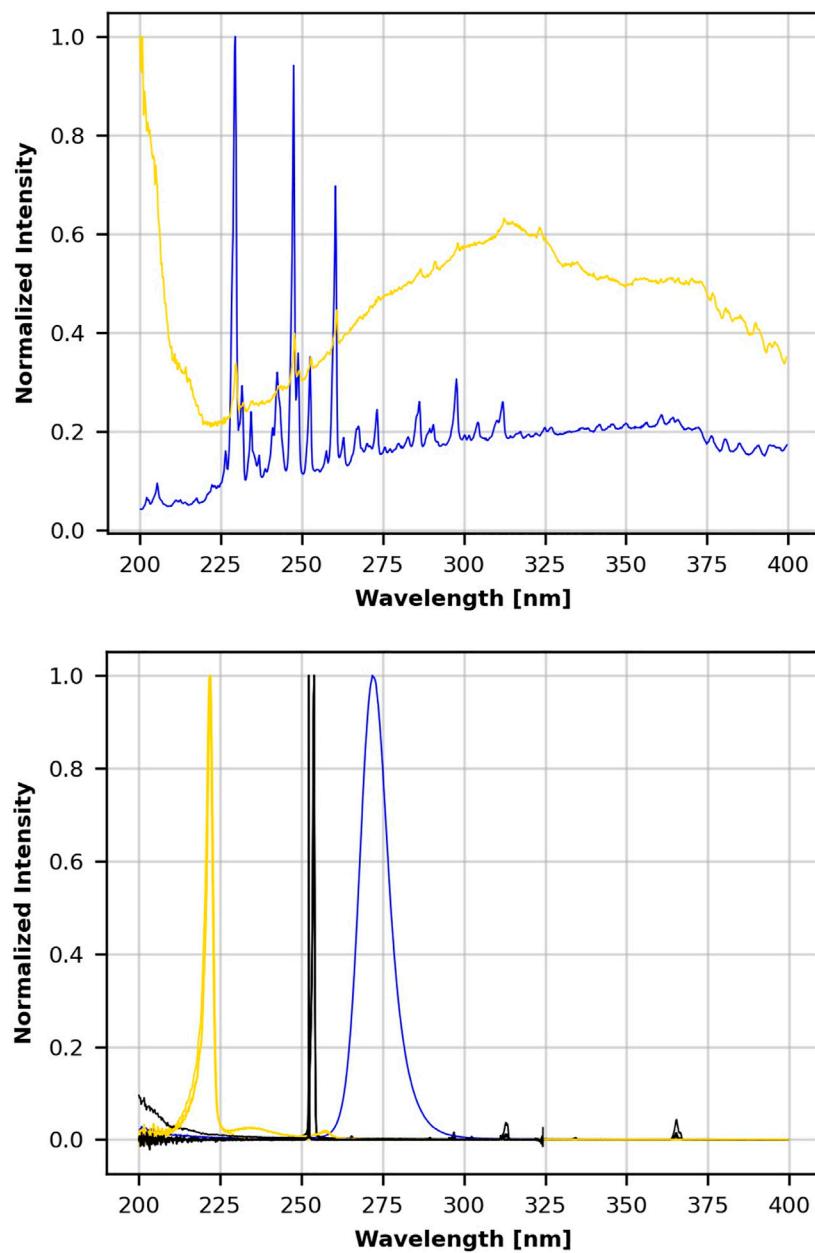


FIGURE 2

Normalized wavelength emission spectra for 14 UV devices. Top frame shows Xenex () and pulsed xenon () emission. Lower frame shows the emission for three 222 nm emitters (), eight 254 nm emitters (), and the 272 nm emitter ().

Results

A focus of this work was to generate information for screening field devices and to provide feedback for iterative product improvement. The emission data for all commercial UV sources are shown and compared in Figure 2. The four handheld devices included 18 and 35 W 254 nm emitters; a 272 nm prototype, and a 222 nm prototype. The five room

devices included Xenex, LEM (254 nm), medium conveyer (254 nm), Big Box (254 nm), and pulsed Xe. The five air/surface prototype devices were prototype A (222 nm), prototype A (254 nm), prototype B (222 nm), prototype B (254 nm), and prototype C (254 nm). The variability of UV emission from different commercial UV sources (Figure 2) was enough by itself to justify the need for high confidence, quantitative, and field test standards to guide product screening

TABLE 1 Average extraction efficiency of $\Phi 6$ virus 4–14 days after drying on different materials.

	PMMA	ABS					
	Plastic	Plastic	Cardboard	NTC	SS304	Polyurethane	Glass
Test days	11	4	16	15	18	9	1
Total samples	55	20	80	75	90	45	5
Extraction %	57.1 \pm 24.2	71.8 \pm 14.6	59.3 \pm 18.7	54.3 \pm 20.0	58.1 \pm 19.9	54.1 \pm 18.8	95.2 \pm 10.2

and iterative improvements in UV devices. Differences in intensity, dosages, and virucidal efficacy among UV sources and devices were additional justifications for standardized field testing that are described later. Data for some prototypes were deliberately omitted since several prototypes were in the process of development with the expectation of future iterative improvements.

Extraction of viable virus from each non-treated control sample demonstrated that the extraction efficiency was consistent across materials for 4–14 days (d) after coupon inoculation with $>8 \log_{10}$ virus and subsequent drying (Table 1). This was an important goal to meet in order to demonstrate that the method could generate reproducible results for tests at multiple field test sites outside of laboratory containment. The selection of materials to be inoculated for different devices was dependent on the intended use of different devices, the iteration of testing, and the availability of different materials, noting that different materials were available at different times during testing because of procurement limitations during COVID-19. After initial virus testing with keyboard keys, flat ABS coupons were procured. The keyboard keys were later identified as PMMA plastic rather than ABS plastic through Fourier transform infrared spectroscopy, although both types of plastics are used for keyboards and both are non-porous, hard plastics.

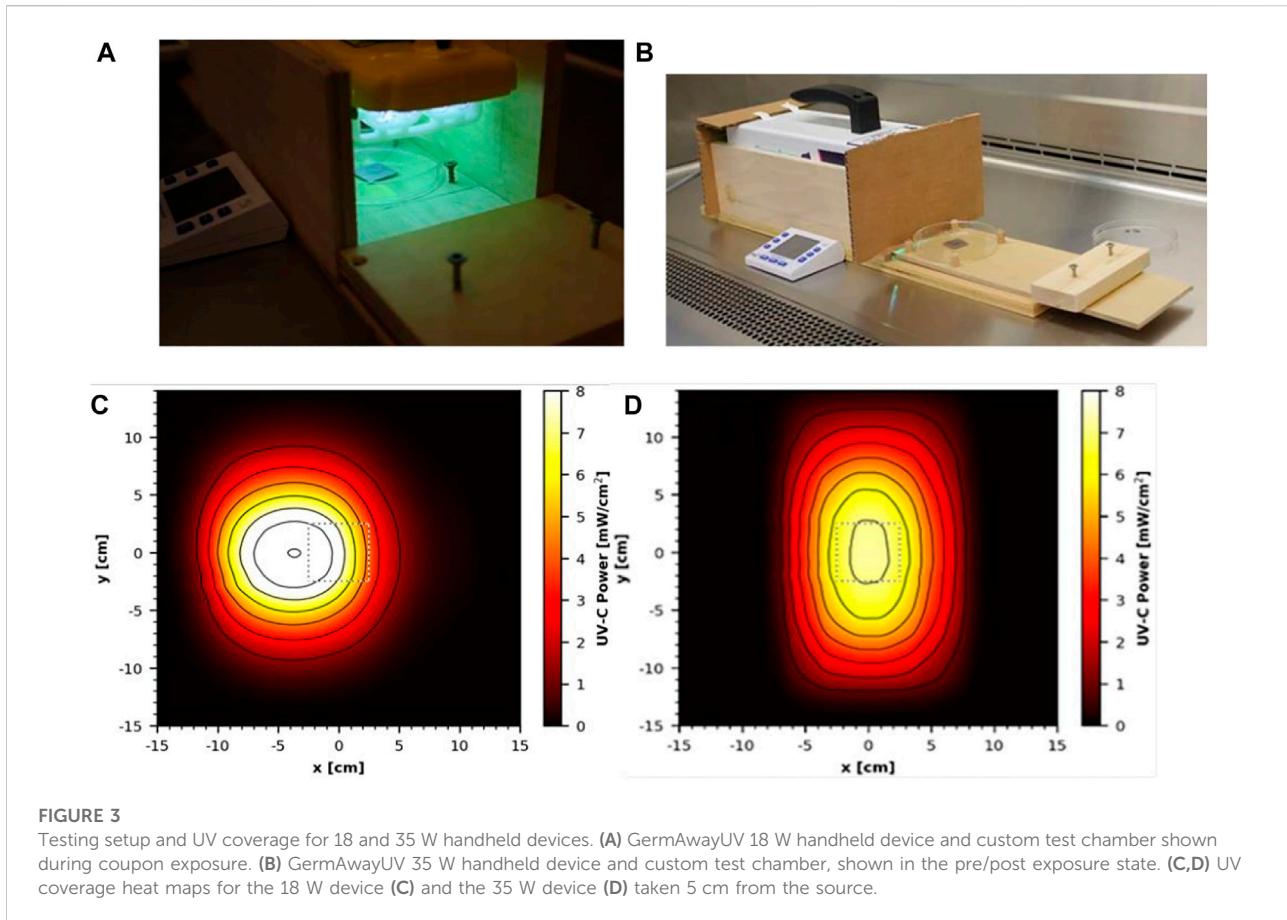
Greater than 1,000 $\Phi 6$ test samples, plus the corresponding $\Phi 6$ -inoculated, non-treated coupon controls, and inoculum controls, were decontamination tested with $\geq 8 \log_{10}$ $\Phi 6$ sample⁻¹ during COVID-19 in both laboratory and field testings (>20 field tests), which included both hot, humid air (Buhr et al., 2020) and this UV testing. A total of 20 independent $\Phi 6$ preparations with a titer of $11 \pm 0.2 \log_{10} \text{ ml}^{-1}$ were generated on different days by 13 different technicians. Five independent virus preparations were tested on each material for each test. A total of 13 technicians were interchangeably used in different steps of the virus quantitation procedure, and 9 technicians were used on a standard high throughput test day. The reproducibility of the test controls across different test days with numerous technicians and with virus extraction that ranged from 4 to 14 days after inoculation demonstrated reproducibility of the test method. Methods reproducibility in this data set was critical because coronavirus test methods and results varied significantly

during COVID-19, which limited the confidence with which to interpret most published data on coronavirus stability and decontamination (Hadi et al., 2020).

Commercial handheld devices (18 W and 35 W)

Two commercial handheld devices were acquired and tested, each within a custom test apparatus. The first was the GermAwayUV 18 W handheld UV-C surface sanitizer (SKU 202110, bulb SKU 195317, CureUV, Delray Beach, FL, United States), a 120 V/60 Hz device containing two 12.7 cm long, U-shaped (Hg) UV bulbs emitting 254 nm UV-C radiation (Figure 3A). An average intensity of 7.61 mW cm^{-2} was measured within a decontamination footprint of $4.47 \text{ cm} \times 5.39 \text{ cm}$ at a 5 cm standoff distance from the bulb (heat map of UV coverage is shown in Figure 3C). The second device was the GermAwayUV Premier 35 W handheld UV-C surface sanitizer (PN14-110-800-100, EPA Product No. 94850-DV-6, CureUV, Delray Beach, FL, United States), 120V/60Hz handheld containing two Hg bulbs that emit 254 nm UV-C radiation, with reflective material positioned within the unit to enhance UV coverage (Figure 3B). The twin tube bulbs spanned a length of 22.5 cm. The 35 W device provided an average intensity of 6.95 mW cm^{-2} at 5 cm standoff distance from the bulb (Figure 3D). The 35 W handheld was later discovered to contain ineffective ballasts (P/N 14-110-800-100), which negatively impacted the results.

For testing the two handheld devices, wooden holding chambers were constructed, in which the devices could be placed to provide standardized exposures to test materials. They were designed to hold the UV source 5 cm above the surface of a test coupon, to prevent UV reflection, and to allow coupons to be inserted into the apparatus *via* a sliding tray for a specified time period of virus inactivation and then promptly removed (Figures 3A). The design of the chambers was the same for the two devices and only varied in size to accommodate the different dimensions of each device. The handheld devices had variable UV output immediately after turning them on. In order to generate consistent dosage for laboratory-to-laboratory testing, the devices were powered on



30 min prior to testing and remained powered on for the duration of the test. Cost and schedule limitations prevented a statistical test among multiple handhelds from different manufacturing batches to assess the variability within and among devices and to determine a minimum warm-up time for end users. The variability highlighted an important gap, dosage monitoring in the field, which needs to be addressed for end users. To prevent potential contamination, the test chambers and devices were wiped down with pH 6.8-adjusted bleach prior to being positioned inside a biosafety cabinet (BSC) for testing.

The sliding tray was constructed to hold a sterile Petri dish *via* guides and included a stop bar to ensure that the sample would be consistently positioned directly under the center of the UV source for maximum exposure. A cardboard barrier was placed over the opening of the chamber to prevent premature UV exposure onto test coupons when the materials were outside the test chamber. The plastic lid was removed from the Petri dish prior to UV exposure, and the dish was wide enough that its edges did not impede UV transmission.

$N = 5$ was tested for each material at each time point. Each of the five coupons was inoculated with an independent virus preparation, emphasizing statistical accuracy over precision,

and three separate exposures were tested for a total $N = 15$. Test chambers held the UV source at a distance of 5 cm from the coupons, with the exception of keyboard keys. The keyboard keys were taller, and the distance from the UV bulb was 4.28–4.38 cm. The 18 and 35 W handheld devices emitted steady state intensities of 10.12 and 6.9 mW cm^{-2} , respectively at the geometric center under the device. Test coupons were exposed to 10 or 20 s (s) of UV-C radiation from the 18 W handheld and 2, 5, or 10 s of UV-C radiation from the 35 W handheld. Different exposure times for the two devices were chosen based on pre-experimental predictions that were considered for practical application of the devices in a field setting. Prior to testing, it was assumed that 35 W radiation would exceed 18 W and 10 s was a common time variable for both 18 and 35 W handhelds. During testing, the ambient environment was $22 \pm 2^\circ\text{C}$ and 40% RH. The surface temperature within the test chamber reached 36°C under the 18 W device and 48°C under the 35 W device. Following UV exposure, coupons were transferred using sterile forceps to 50-ml conical tubes for extraction. The corresponding virus-inoculated control coupons were left under ambient conditions during testing because prior testing with $\Phi 6$ showed complete recovery/survival of $>8 \log_{10}$ of dried virus after treatment of different surfaces at 55°C , 50% RH for

TABLE 2 Dosage and efficacy of handheld, room, and chamber-type devices showing \log_{10} reduction data based on the steady-state emission, not peak emission. White (low decontamination) = Fail $<2 \log_{10}$; yellow (sanitation) = Fail $\geq 2 \log_{10}$, $<3 \log_{10}$; light blue (disinfection) = Pass $\geq 3 \log_{10}$; and dark blue (approaching virus sterilization) = Pass $\geq 6 \log_{10}$. N/A—dosage measurements had no meaning because of the broad-spectrum Xe source.

Name	Description	Dosage (mJ cm ⁻²)	Exposure distance	Exposure time	Efficacy (\log_{10} reduction after an $>8 \log_{10}$ challenge of live $\Phi 6$)				
					SS304	NTC	Cardboard	^a PMMA or ABS plastic	Polyurethane
GermAwayUV 18 W handheld	Two 12.7 cm Hg U-shape bulbs in the handheld device 254 nm UV-C MSRP \$100	101.2	5 cm	10 s	2.5 ± 0.1	2.0 ± 0.0	1.9 ± 0.0	1.9 ± 0.0	2.0 ± 0.0
		202.4	5 cm	20 s	4.3 ± 0.2	3.1 ± 0.2	2.0 ± 0.1	4.5 ± 0.1	3.3 ± 0.1
GermAway UV 35 W handheld	Two 22.5 cm Hg twin tube bulbs in the handheld device 254 nm UV-C MSRP \$450	13.8	5 cm	2 s	0.3 ± 0.0	0.2 ± 0.0	0.3 ± 0.0	0.3 ± 0.0	0.3 ± 0.0
		34.5	5 cm	5 s	0.9 ± 0.1	0.6 ± 0.0	0.7 ± 0.0	0.8 ± 0.1	0.7 ± 0.0
		69.0	5 cm	10 s	1.4 ± 0.1	1.2 ± 0.1	1.2 ± 0.0	1.3 ± 0.0	1.1 ± 0.1
272 nm prototype handheld	Eight LED strips divided by angled plastic in the handheld device 272 nm UV-C	31.2	5 cm	2 s	3.0 ± 0.3	1.6 ± 0.2	1.6 ± 0.1	1.6 ± 0.2	1.6 ± 0.2
		78.0	5 cm	5 s	5.2 ± 0.1	2.8 ± 0.1	2.5 ± 0.2	3.1 ± 0.2	2.0 ± 0.9
		156	5 cm	10 s	6.2 ± 0.4	3.8 ± 0.2	2.4 ± 0.1	4.9 ± 0.2	4.7 ± 0.5
222 nm excimer prototype handheld	Three lamp modules attached to 2.54 cm thick plastic panel, in the handheld device 222 nm UV-C	5.9	5 cm	2 s	0.6 ± 0.1	0.4 ± 0.2	0.1 ± 0.1	0.3 ± 0.1	0.3 ± 0.1
		14.8	5 cm	5 s	0.9 ± 0.2	0.1 ± 0.1	0.5 ± 0.1	0.5 ± 0.1	0.6 ± 0.2
		29.6	5 cm	10 s	1.1 ± 0.2	0.9 ± 0.1	0.6 ± 0.1	0.9 ± 0.1	1.1 ± 0.1
Mounted pulsed- xenon prototype	Pulsed Xe bulb in small housing ceiling, wall, or tripod-mounted broad-spectrum UV-B and UV-C	N/A	0.5 m	15 min	1.4 ± 0.1	1.1 ± 0.1	1.1 ± 0.1	1.5 ± 0.1	N/A
			0.5 m	30 min	2.3 ± 0.1	2.3 ± 0.1	1.6 ± 0.1	2.9 ± 0.1	N/A
			0.5 m	60 min	5.2 ± 0.2	3.2 ± 0.3	2.4 ± 0.2	5.2 ± 0.2	N/A
			1 m	15 min	0.5 ± 0.0	0.4 ± 0.1	0.4 ± 0.1	0.3 ± 0.1	N/A
			1 m	30 min	0.8 ± 0.0	0.7 ± 0.0	0.7 ± 0.1	0.7 ± 0.0	N/A
			1 m	60 min	1.5 ± 0.1	1.3 ± 0.1	1.0 ± 0.0	1.3 ± 0.1	N/A
			2 m	15 min	0.0 ± 0.1	0.1 ± 0.1	0.2 ± 0.0	0.1 ± 0.0	N/A
			2 m	30 min	0.1 ± 0.0	0.0 ± 0.0	0.2 ± 0.0	0.2 ± 0.1	N/A
			2 m	60 min	0.3 ± 0.0	0.2 ± 0.1	0.3 ± 0.0	0.2 ± 0.0	N/A
Xenex LightStrike	One pulsed Xe bulb mounted on the rolling cart broad-spectrum UV-B and UV-C MSRP \$125,000	N/A	178 cm	5 min	0.8 ± 0.1	0.4 ± 0.0	0.5 ± 0.0	0.5 ± 0.0	N/A
		N/A	178 cm	20 min	1.7 ± 0.0	1.5 ± 0.1	1.3 ± 0.0	2.2 ± 0.1	NA
Light emitting module (LEM)	20 Hg bulbs mounted in a ring on the rolling cart 254 nm UV-C MSRP \$95,000	60	263 cm	4 min 22 s	3.1 ± 0.3	2.6 ± 0.2	1.6 ± 0.1	2.5 ± 0.2	2.1 ± 0.1
		100	263 cm	7 min 2 s	4.6 ± 0.5	2.7 ± 0.2	2.2 ± 0.1	2.7 ± 0.2	3.1 ± 0.1
		140	263 cm	9 min 33 s	5.3 ± 0.5	3.4 ± 0.1	2.7 ± 0.1	4.0 ± 0.2	3.9 ± 0.1
Medium conveyer prototype	Chamber lined on four sides with Hg bulbs and powered conveyer belt to move items through 254 nm UV-C	60	62 cm	20 s	6.1 ± 0.2	4.5 ± 0.1	2.9 ± 0.3	4.8 ± 0.2	5.3 ± 0.1
		100	62 cm	32 s	7.6 ± 0.3	4.4 ± 0.2	2.9 ± 0.2	6.3 ± 0.2	7.1 ± 0.3
		140	62 cm	44 s	7.1 ± 0.4	4.3 ± 0.5	2.6 ± 0.1	6.3 ± 0.3	6.3 ± 0.3
		13.7	62 cm	8 s	1.6 ± 0.2	1.4 ± 0.1	1.3 ± 0.1	1.4 ± 0.1	N/A
		23.8	62 cm	16 s	2.7 ± 0.2	1.9 ± 0.1	1.8 ± 0.1	2.1 ± 0.1	N/A
		40.0	62 cm	24 s	3.5 ± 0.3	2.8 ± 0.1	2.5 ± 0.1	2.9 ± 0.1	N/A
	56.2	62 cm	32 s	4.7 ± 0.4	3.2 ± 0.2	2.9 ± 0.1	3.7 ± 0.1	N/A	
Big box prototype	Chamber lined on sides and top with Hg bulbs (total 320) 254 nm UV-C	377–729	17 cm	2 min	5.4 ± 0.2	3.6 ± 0.3	3.1 ± 0.2	5.7 ± 0.1	5.4 ± 0.3

^aABS plastic was tested for the mounted pulsed Xe and Big Box prototypes. PMMA plastic was tested for the other devices.

1 h (Buhr et al., 2020). Of note, wet virus was completely killed at 55°C, 50% RH for 1 h (Buhr et al., 2020), and an important data point that supported the goal for testing dried virus is described in the introduction and discussion. Hence, the heat (48°C) could have potentially impacted decontamination kinetics if the tests had used wet virus instead of dried virus. The UV test parameters here were of short duration (up to 10 s) and the surface temperatures likely did not equilibrate much above ambient temperature. Importantly, the high temperatures measured under these handhelds generates a practical risk for the end users because it is not known if the heat generated might create a fire hazard if the lamps are left on for extended periods. While 48°C was the highest temperature measured among any of the devices, temperature measurements over extended run periods for multiple different handheld batches would be needed for safety assessments prior to field use, and this task was outside of the testing scope.

The dosage and virus inactivation results are summarized in Tables 2 (\log_{10} reduction) and 3 (\log_{10} survival). Dosages and virus inactivation were measured at a 5 cm distance, which was considered a reasonable, practical distance for a handheld device used to scan over surfaces. The keyboard keys were slightly taller and closer to the UV source. Thus, the dosage on the keys was slightly greater than that on the other materials, but no dosage calculations were made specifically for those keys.

To evaluate the efficacy of the devices, a minimum of 3 \log_{10} inactivation was targeted, which is equivalent to a 99.9% reduction and corresponds to the current EPA requirements for chemical disinfection. A 10 s exposure with the GermAway 18 W unit failed to meet the $\geq 3 \log_{10}$ inactivation threshold for all tested materials. A 20 s exposure successfully achieved a greater than 3 \log_{10} inactivation out of an 8.2 \log_{10} virus challenge on SS304, NTC, keyboard keys, and polyurethane but failed to meet the 3 \log_{10} inactivation threshold on cardboard.

The GermAwayUV 35 W handheld sanitizer failed to meet the $\geq 3 \log_{10}$ inactivation threshold out of an 8 \log_{10} PFU virus challenge on all five materials for all three exposure durations, achieving less than 2 \log_{10} PFU inactivation. The GermAwayUV 35 W handheld sanitizer delivered lower dosage than the 18 W handheld despite nearly double the power. Hence there was no correlation between power and dosage/efficacy, and the importance of measuring every device was apparent.

Prototype handheld devices (272 nm light emitting diodes and 222 nm lamp modules)

Two additional handheld devices were tested for efficacy of virus inactivation, which were prototypes rather than commercial units. The first prototype was one of two custom 3-D printed proprietary units and featured eight LED strips, which emitted 272 nm wavelength UV-C radiation. The face of

the handheld was 320 mm \times 100 mm, with the LED strips covering 255 mm \times 60 mm. An average intensity of 12.71 mW cm^{-2} was measured within a decontamination footprint of 6 cm \times 25.5 cm at 5 cm standoff distance from the bulb (Figures 4A). The second prototype device utilized three 222 nm UV-C excimer lamp modules installed into a 2.54 cm thick white plastic panel with power supply. It is important to note that this was strictly an early prototype undergoing iterative improvements, and the UV sources were spaced too far from a wand configuration. An average intensity of 1.54 mW cm^{-2} was measured at 5 cm standoff distance from an individual module (Figures 5A).

The test chambers for the prototype handhelds followed the same design as those for the 18 and 35 W devices, with the additional feature of a wooden barrier that removed the need for cardboard to prevent premature UV exposure onto test coupons when the materials were outside the UV chamber. Again, there was a 5 cm vertical standoff distance from the UV source to the surface of the test coupons. Mimicking the 18 and 35 W handheld unit tests, the devices were powered on 30 min prior to testing to warm up and remained powered on for the duration of the test. An Ophir Spiricon Starbright Dosimeter (S/N 949,685, P/N 7,201,580) and sensor (S/N 954,282, P/N 7Z02479) were used to confirm that the 222 nm device was on and emitting 222 nm UV radiation, as the design of the prototype did not allow visual confirmation that the device was on after it was plugged in. The test chambers and handheld UV devices were wiped down with pH 6.8-adjusted bleach prior to being positioned inside a BSC for testing.

$N = 5$ coupons for each material were tested at each time/dosage with each coupon inoculated with an independent virus preparation. During tests, virus-inoculated coupons were transferred one-by-one to sterile Petri plates and inserted into the test chambers *via* the sliding tray for timed UV exposures at the geometric center of the handheld device. For the 272 nm device, the cardboard coupons were anchored down using sterile pipette tips due to the large amount of air movement generated by the cooling fans of the device. In the 272 nm prototype, coupons were exposed to a steady state intensity of 15.6 mW cm^{-2} measured at the geometric center of the device with a 5 cm standoff distance. Similarly, the 222 nm prototype emitted an intensity of 2.96 mW cm^{-2} at a similar location centered under a single-lamp module. Following UV exposure, the coupons were transferred to 50-ml conical tubes for extraction. For both devices, test coupons were exposed to UV-C radiation for 2, 5, or 10 s. For the 272 nm device, the ambient environment during testing was $21 \pm 2^\circ\text{C}$ and 21% RH, and the surface temperature under the sterilizer reached $34.7 \pm 2^\circ\text{C}$. For the 222 nm device, the ambient environment was $21.8 \pm 2^\circ\text{C}$ and 20% RH, and the surface temperature reached $28.3 \pm 2^\circ\text{C}$ within the test chamber.

The dosage and virus inactivation results are summarized in Tables 2 (\log_{10} reduction) and 3 (\log_{10} survival). The 272 nm LED prototype successfully achieved a $\geq 3 \log_{10}$ PFU inactivation

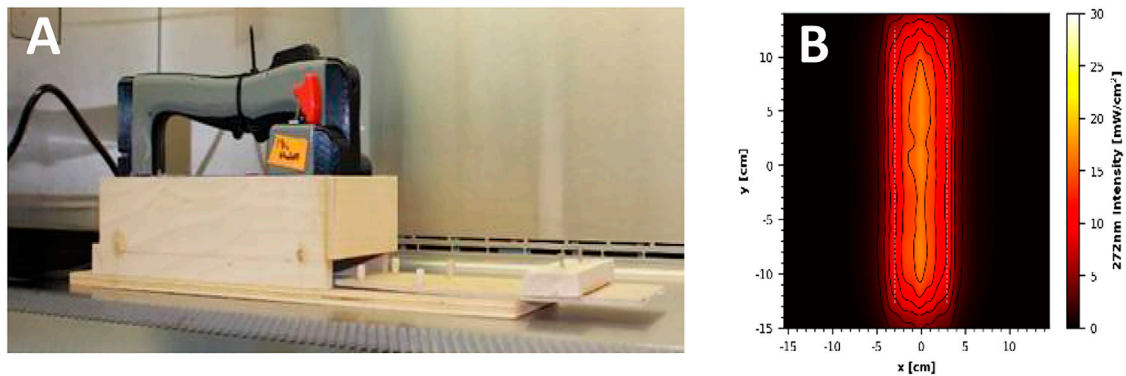


FIGURE 4
(A) Prototype 272 nm LED handheld inside the wooden test chamber. (B) UV coverage heat map taken 5 cm from the source.

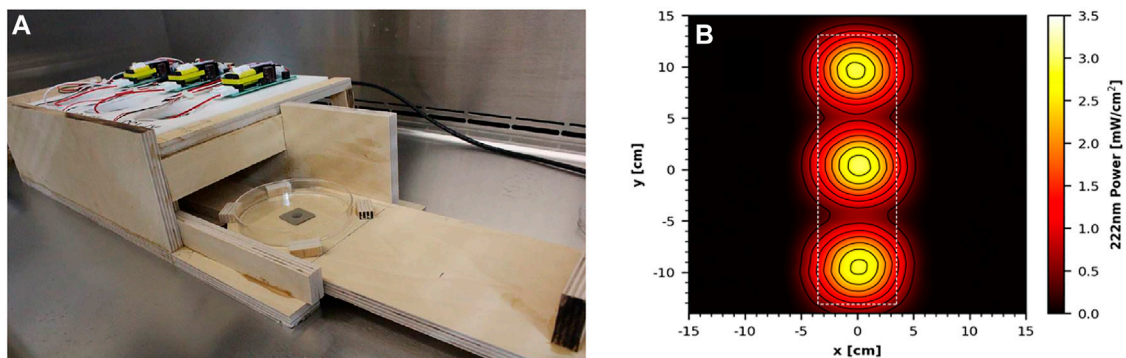


FIGURE 5
(A) Prototype 222 nm Excimer Lamp Module Board inside the wooden test chamber. (B) UV coverage heat map taken 5 cm from the source.

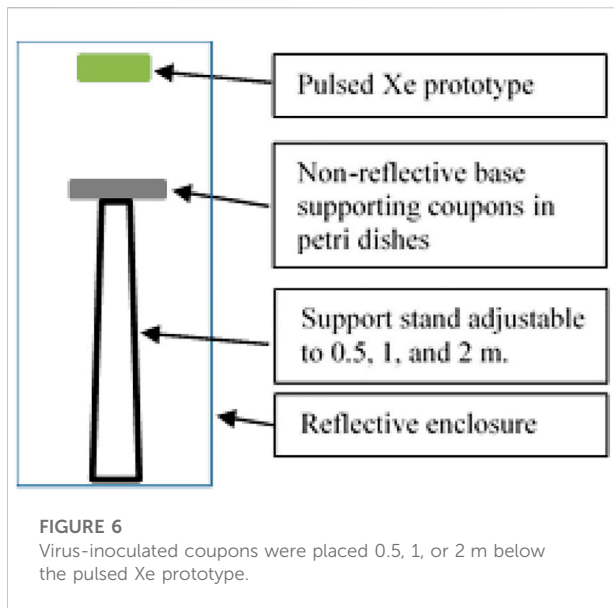
out of an $8.5 \log_{10}$ PFU virus challenge for SS304 at 2, 5, and 10 s, for ABS at 5 and 10 s, and for NTC and polyurethane at 10 s. The hardest, smoothest material was SS304, and it showed the greatest \log_{10} reduction at all three time points. Cardboard showed the lowest inactivation rate with no treatments providing $\geq 3 \log_{10}$ PFU inactivation. Overall, the 272 nm LED prototype showed significantly greater virus inactivation compared to the 18 and 35 W handheld commercial devices.

The 222 nm excimer UV prototype failed to achieve a $>3 \log_{10}$ inactivation out of an $8.5 \log_{10}$ virus challenge for all five materials tested, making it the least effective of the four handheld devices tested. Further testing with longer exposure times might produce results passing the $\geq 3 \log_{10}$ inactivation threshold. From a practical standpoint, these data showed that this 222 nm prototype had poor efficacy and very limited utility. Since this was a prototype, iterative improvements can be made to improve performance of this device.

Prototype mounted pulsed xenon unit for room decontamination

A prototype room decontamination unit featuring a pulsed Xe UV bulb was tested. The unit consists of a pulsed Xe bulb within a frame intended to be mounted onto a wall, ceiling, or mobile tripod for room decontamination. The UV source emitted a small burst of broad spectrum radiation every 6 s, with the burst lasting for a short duration. The electromagnetic spectrum included UV-C, UV-B, UV-A, and violet-blue visible radiation. The reflector material was positioned behind the source to enhance UV output.

Testing of the modified prototype took place within an enclosure provided by the vendor. The device was mounted at 0.5, 1, and 2 m vertical standoff distance above the testing surface (Figure 6). Test coupons were placed below the prototype in sterile Petri dishes, and an aseptic technique was employed to the greatest extent possible while outside of a BSC to prevent

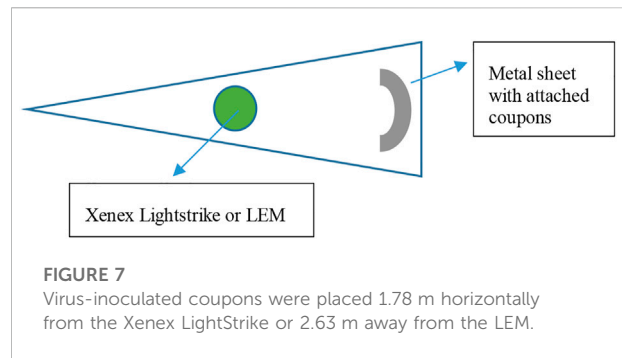


contamination. The coupons contained within Petri dishes were uncovered just prior to the test and re-covered at the conclusion of the exposure times. Independent tests were run for three exposure times (15, 30, and 60 min), each taken at 0.5, 1, and 2 m distances from the UV source. These time increments were determined *via* the recommended cycle lengths from the vendor and corresponded to vendor test data (30 and 60 min only). The device was pre-programmed for 30 min run times, therefore for the 15-min increment, coupons were removed from the enclosure without shutting off the device after 15 min had elapsed from the time of the first flash. For the 60-min cycle, two decontamination cycles were run sequentially.

Results for a mounted prototype containing a pulsed Xe bulb are shown in Tables 2 (\log_{10} reduction) and 3 (\log_{10} survival). This device emitted broad spectrum radiation in pulses occurring every 6 s with the duration of each pulse measured at 0.489 s, and the majority of the dosage applied over the first few milliseconds of that time. Because of the broad spectrum nature, the UV dosage could not be confidently measured. This device demonstrated measurable efficacy at 0.5 m for 60 min, and the results were best on non-porous materials. The efficacy was very limited at 1 and 2 m and shorter exposure times, particularly on porous cardboard, followed by semi-porous NTC. As usual, the best efficacy was on smooth surfaces: plastic and SS304.

Commercial rolling units for room decontamination

Two commercial rolling units designed for room decontamination were purchased. The first was the Xenex LightStrike (Model PXUV4D, S/N 002,628, Xenex Disinfection



Systems, San Antonio, TX, United States), which contained one pulsed Xe bulb (broad spectrum across the germicidal spectrum of 200–315 nm). The bulb extends and retracts at the top of the unit and pulsed at a rate of 67 flashes per s. The intensities and dosages at specific wavelengths were not carefully analyzed/dissected because the work was not aimed at correlating specific wavelength dosages from a broad spectrum device to a kill rate. The second unit was the light emitting module (“LEM,” Rapid UV-C Disinfection Model R3, S/N 473, 120V/12A, STERILIZ, LLC, 150 Linden Oaks, Rochester, NY 14625–2,802), which contained a ring of 20 Hg bulbs with a 41-cm diameter that emitted predominantly 254 nm wavelength UV-C radiation. The device was tested at an exposure distance of 2.63 m from the center of the Hg bulb ring (Figure 7). The length of exposure was controlled based upon the cumulative dosage recorded *via* LEM system dosimeters placed next to the test coupons and targeted for exposures of 60, 100, and 140 mJ cm^{-2} . Coupons were exposed to an average intensity calculated to be 0.23–0.24 mW cm^{-2} . Due to the different expected intensities of the UV sources, the devices were set at different distances from test coupons to achieve similar dosages in an attempt to directly compare the killing efficacy of a broad spectrum radiation source to a 254 nm source.

For testing, the Xe or Hg rolling units were positioned in the corner of a triangular area, and non-reflective folding panels were set up to prevent UV exposure to personnel outside of the decontamination area. Magnets were glued to the underside of test coupons prior to inoculation of virus, and a black, non-reflective, metal sheet rack was utilized as a support for the test coupons. The rack was bent into a curved shape in an attempt to maintain a constant UV exposure distance to all coupons. Testing of these two devices required transport of coupons to the testing site, and coupons were transported in 50-ml conical tubes at room temperature. Negative control coupons and additional shipping controls (inoculated and transported, but not exposed to UV) were also included. Conditions in the testing room were not aseptic but care was taken to avoid contamination at each step and coupons were only transferred to and from the metal rack using sterile forceps. After UV exposure, the samples were transferred to new sterile conical tubes and transported

TABLE 3 Dosage and efficacy of handheld, room, and chamber-type devices showing log₁₀ survival data based on the steady state emission, not peak emission. White (low decontamination) = Fail <2 log₁₀; yellow (sanitation) = Fail ≥2 log₁₀, <3 log₁₀; light blue (disinfection) = Pass ≥3 log₁₀; and dark blue (approaching virus sterilization) = Pass ≥6 log₁₀. N/A—dosage measurements had no meaning because of the broad-spectrum Xe source.

Name	Description	Dosage (mJ cm ⁻²)	Exposure distance	Exposure time	Log ₁₀ survival after a >8 log ₁₀ challenge of live Φ6					
					Inoculum	SS304	NTC	Cardboard	^a PMMA or ABS plastic	Polyurethane plastic
GermAwayUV 18 W handheld	Two 12.7 cm U-shape Hg bulbs in the handheld device 254 nm UV-C MSRP \$100	101.2	5 cm	10 s	8.4 ± 0.1	5.9 ± 0.5	6.4 ± 0.1	6.5 ± 0.1	5.5 ± 1.1	6.4 ± 0.1
		202.4	5 cm	20 s	8.2 ± 0.0	3.9 ± 0.4	5.0 ± 0.4	6.1 ± 0.3	3.7 ± 0.3	5.1 ± 0.2
GermAway UV 35 W handheld	Two 22.5 cm twin tube Hg bulbs in the handheld device 254 nm UV-C MSRP \$450	13.8	5 cm	2 s	8.2 ± 0.1	7.8 ± 0.2	7.9 ± 0.1	7.8 ± 0.1	7.8 ± 0.2	7.8 ± 0.1
		34.5	5 cm	5 s		7.2 ± 0.2	7.5 ± 0.1	7.3 ± 0.1	7.3 ± 0.3	7.4 ± 0.1
		69.0	5 cm	10 s		6.6 ± 0.3	6.9 ± 0.2	6.9 ± 0.1	6.8 ± 0.2	7.0 ± 0.2
272 nm prototype handheld	Eight LED strips divided by angled plastic in the handheld device 272 nm UV-C	31.2	5 cm	2 s	8.5 ± 0.2	5.5 ± 0.6	7.0 ± 0.3	6.9 ± 0.2	6.9 ± 0.3	6.9 ± 0.4
		78.0	5 cm	5 s		3.3 ± 0.0	5.7 ± 0.1	6.0 ± 0.4	5.4 ± 0.3	6.5 ± 1.9
		156	5 cm	10 s		2.3 ± 0.7	4.7 ± 0.3	6.1 ± 0.1	3.6 ± 0.5	3.8 ± 0.9
222 nm excimer prototype handheld	Three lamp modules attached to 2.54 cm thick plastic panel, in the handheld device 222 nm UV-C	5.9	5 cm	2 s	8.3 ± 0.2	7.7 ± 0.2	7.9 ± 0.3	8.2 ± 0.1	8.0 ± 0.1	7.9 ± 0.0
		14.8	5 cm	5 s		7.4 ± 0.3	8.2 ± 0.1	7.8 ± 0.1	7.8 ± 0.2	7.6 ± 0.3
		29.6	5 cm	10 s		7.1 ± 0.4	7.1 ± 0.4	7.6 ± 0.1	7.4 ± 0.2	7.1 ± 0.1
Mounted pulsed xenon prototype	Pulsed Xe bulb in small housing ceiling, wall, or tripod-mounted broad-spectrum UV-B and UV-C	N/A	0.5 m	15 min	8.2 ± 0.1	6.8 ± 0.2	7.0 ± 0.2	7.1 ± 0.2	6.7 ± 0.1	N/A
			0.5 m	30 min		5.9 ± 0.3	5.8 ± 0.3	6.6 ± 0.1	5.3 ± 0.2	N/A
			0.5 m	60 min		2.9 ± 0.4	5.0 ± 0.8	5.7 ± 0.5	3.0 ± 0.6	N/A
			1 m	15 min		7.7 ± 0.1	7.7 ± 0.2	7.7 ± 0.1	7.8 ± 0.1	N/A
			1 m	30 min		7.4 ± 0.1	7.5 ± 0.0	7.4 ± 0.1	7.4 ± 0.1	N/A
			1 m	60 min		6.7 ± 0.2	6.8 ± 0.2	7.2 ± 0.1	6.8 ± 0.2	N/A
			2 m	15 min		8.2 ± 0.1	8.1 ± 0.1	8.0 ± 0.1	8.1 ± 0.0	N/A
			2 m	30 min		8.1 ± 0.1	8.1 ± 0.1	8.0 ± 0.1	8.0 ± 0.1	N/A
Xenex LightStrike	One pulsed-Xe bulb mounted on the rolling cart broad-spectrum UV-B and UV-C MSRP \$125,000	N/A	178 cm	5 min	8.4 ± 0.0	7.6 ± 0.2	8.0 ± 0.1	7.9 ± 0.1	7.8 ± 0.1	N/A
		N/A	178 cm	20 min		6.7 ± 0	6.9 ± 0.3	7.1 ± 0.0	6.2 ± 0.1	N/A
Light emitting module (LEM)	20 Hg bulbs mounted in a ring on the rolling cart 254 nm UV-C MSRP \$95,000	60	263 cm	4 min 22 s	8.4 ± 0.2	5.3 ± 0.6	5.8 ± 0.5	6.8 ± 0.2	5.9 ± 0.5	6.3 ± 0.1
		100	263 cm	7 min 2 s		3.8 ± 1.1	5.7 ± 0.5	6.2 ± 0.2	5.7 ± 0.4	5.3 ± 0.1
		140	263 cm	9 min 33 s		3.1 ± 1.1	5.0 ± 0.3	5.8 ± 0.2	4.4 ± 0.3	4.6 ± 0.2
Medium conveyer prototype	Chamber lined on four sides with Hg bulbs and powered conveyer belt to move items through 254 nm UV-C	60	62 cm	20 s	8.2 ± 0.1	2.1 ± 0.4	3.7 ± 0	5.3 ± 0.6	3.4 ± 0.4	2.9 ± 0.1
		100	62 cm	32 s		0.6 ± 0.6	3.8 ± 0.5	5.3 ± 0.4	2.0 ± 0.4	1.1 ± 0.7
		140	62 cm	44 s		1.1 ± 0.8	3.9 ± 1.1	5.6 ± 0.1	1.9 ± 0.6	0.9 ± 0.5

(Continued on following page)

TABLE 3 (Continued) Dosage and efficacy of handheld, room, and chamber-type devices showing log₁₀ survival data based on the steady state emission, not peak emission. White (low decontamination) = Fail <2 log₁₀; yellow (sanitation) = Fail ≥2 log₁₀; <3 log₁₀; light blue (disinfection) = Pass ≥3 log₁₀; and dark blue (approaching virus sterilization) = Pass ≥6 log₁₀. N/A—dosage measurements had no meaning because of the broad-spectrum Xe source.

Name	Description	Dosage (mJ cm ⁻²)	Exposure distance	Exposure time	Log ₁₀ survival after a >8 log ₁₀ challenge of live Φ6					
					Inoculum	SS304	NTC	Cardboard	PMMA or ABS plastic	Polyurethane
		13.7	62 cm	8 s	8.4 ± 0.2	6.8 ± 0.4	7.0 ± 0.1	7.1 ± 0.1	7.0 ± 0.1	N/A
		23.8	62 cm	16 s		5.6 ± 0.4	6.5 ± 0.1	6.5 ± 0.2	6.3 ± 0.1	N/A
		40.0	62 cm	24 s		4.8 ± 0.6	5.5 ± 0.2	5.8 ± 0.3	5.4 ± 0.2	N/A
		56.2	62 cm	32 s		3.7 ± 1.0	5.1 ± 0.4	5.5 ± 0.2	4.7 ± 0.1	N/A
Big box prototype	Chamber lined on sides and top with Hg bulbs (total 320) 254 nm UV-C	377–729	17 cm	2 min	8.4 ± 0.1	3.0 ± 0.4	4.8 ± 0.6	5.3 ± 0.5	2.5 ± 0.3	3.0 ± 0.6
					8.2 ± 0.1 (ABS plastic only)					

^aABS plastic was tested for the mounted pulsed Xe and the Big Box prototypes. PMMA plastic was tested for the other devices.

back to the microbiology laboratory for virus extraction and quantification.

Specific testing conditions differed slightly between the two rolling units. For testing the Xenex LightStrike, the metal stand holding virus-inoculated test coupons was placed such that the coupon height was between 1.09 and 1.55 m above the ground (approximately parallel to the height of the pulsed Xe bulb), and the distance between the coupons and the UV source was 1.72–1.78 m. Based on preliminary dosage readings, the Xenex LightStrike did not need a 30-min warm-up time. Two time points of 5 and 20 min were tested. Room conditions were measured at 23.3 ± 1°C and 74% RH for the first exposure and 25.1 ± 1°C and 22% RH for the second exposure. As the tests occurred in succession approximately 30 min apart, the shift in environmental conditions with the rise in temperature and drop in humidity is speculated to be driven by the Xe unit itself. In addition, the smell of ozone was detected in the air following the completion of each test. The ozone level in the room was measured at 0.26 ppm for the Xenex LightStrike (0.1 ppm is the 8-h occupational safety and health assessment (OSHA) limit).

For testing the LEM, the metal stand holding virus-inoculated test coupons was placed such that the coupon height was approximately 1.2 m above the ground (parallel to center of the Hg bulbs), and the distance between the center of the ring of UV bulbs to the center of the metal arc with coupons was approximately 2.62 m. The distance between the test coupons and the nearest UV bulb was 2.43 m. Testing for this device included three independent exposures of 60, 100, and 140 mJ cm⁻², which took 4 min 22 s, 7 min 2 s, and 9 min 33 s, respectively. The exposure conditions were 26 ± 1°C, 38% RH. The ozone level in the room was measured at 0.08 ppm for the LEM (0.1 ppm is the 8-h occupational safety and health assessment (OSHA) limit).

Results for the Xenex LightStrike unit with pulsed Xe UV bulb are shown in Tables 2, 3. The Xenex LightStrike failed to achieve a ≥3 log₁₀ inactivation out of an 8.4 log₁₀ PFU virus challenge for all five materials tested. One positive is that the Xenex did not require a warm-up time in contrast to devices with Hg bulbs.

Results for the LEM with Hg bulbs are shown in Tables 2, 3. The LEM successfully achieved a ≥3 log₁₀ PFU inactivation out of an 8.4 log₁₀ PFU virus challenge for SS304 at all three dosages, for polyurethane at the higher two exposures, and for NTC and keyboard keys at the highest dosage only. It failed to meet the ≥3 log₁₀ PFU inactivation threshold for cardboard at all three exposure levels.

Prototype medium conveyer

The prototype medium conveyer featured a chamber measuring 2.03 m long × 0.78 m wide × 0.69 m tall that was lined on all interior surfaces with UV-C-emitting (254 nm) Hg

bulbs, including below the powered rollers (Figure 8). Testing of this device required transport of coupons to the testing site, and coupons were transported in 50-ml conical tubes at room temperature. Negative control coupons and additional shipping controls (inoculated and transported, but not exposed to UV) were also included.

Two rounds of testing were performed with the conveyor device, with slight differences in experimental setup and UV dosages. For both rounds, dosimeters were first used in trial-and-error runs to determine the required run-through time to reach the target UV exposures. The dosimeters used were Roithner LaserTechnick GmbH GIVA-S12SD dosimeters from Vienna, Austria, with dimensions of 4.3 cm × 3.5 cm × 1.8 cm. In the first round of experiments, three dosimeters were horizontally taped to a 2% polyethylene board (46.7 cm × 28.6 cm × 2.54 cm) and were sent through the conveyor to get dosage readings based on exposure time (Figure 8). After target exposure times were determined, coupons were placed inside sterile Petri dishes and set on the same polyethylene support board before exposure in the conveyor. The first round of testing included exposures of 60 (22 s), 100 (32 s), and 140 mJ cm⁻² (44 s). Conditions within the conveyor for this round were 27.7°C, 63.2% RH, 0.09 ppm ozone.

In the second round of testing, the initial runs were again dosimeter only to determine exposure times to reach the targeted UV dosages. The same dosimeters were used, but this time, they were placed on a ceramic tile (~45.7 cm × 45.7 cm). During testing, coupons were placed directly on the ceramic tile support to prevent the sides of the Petri dishes from blocking any UV radiation from reaching the coupons. Test conditions were 17.3 ± 1°C and 20.1% RH. Ozone reading was not captured since the ozone reader was unavailable.

Two rounds of testing were carried out for the prototype medium conveyor with Hg bulbs, with each round varying in dosages tested and in the method of exposing the test coupons. The dosages over time were not perfectly linear. The dosage variability over time might have variability in dosimeter readings and/or variability in Hg bulb dosages after warm up. Test results are shown in Tables 2, 3. During round 1 testing at 60 (20 s), 100 (32 s), and 140 mJ cm⁻² (44 s), the conveyor successfully achieved a ≥3 log₁₀ PFU inactivation out of an 8.2 log₁₀ PFU virus challenge for all three exposure times on SS304, NTC, ABS plastic, and polyurethane, with slightly higher inactivation results for ABS plastic and polyurethane at the higher two treatments. It failed to meet the ≥3 log₁₀ PFU inactivation threshold on cardboard for all three exposure times.

For round 2 of testing, the dosages measured during testing were 13.7 (8 s), 23.8 (16 s), 40.0 (24 s), and 56.2 mJ cm⁻² (32 s). Regardless of dosage variability, the conveyor successfully achieved a ≥3 log₁₀ inactivation out of an 8.4 log₁₀ virus challenge for SS304 at 24 and 32 s, for NTC at 32 s, and for ABS plastic at 32 s time points. For all other materials and round

2 exposure times, it failed to reach the ≥3 log₁₀ PFU threshold inactivation.

The conveyor produced UV dose-dependent inactivation at lower dosages (13.7–56.2 mJ cm⁻²), but inactivation leveled off across all surfaces tested at higher dosages (60–140 mJ cm⁻²). The size of the shielded virus population was dependent on material porosity since the highest level of inactivation was observed on non-porous SS304, followed by polyurethane, ABS plastic, NTC, and then porous cardboard. In addition, a sub-population of virus protected by debris was shielded from exposure to radiation because of the presence of host cell debris as indicated by a flattening of the kill rate across all the materials including smooth SS304. That sub-population of debris-complexed virus manifest may manifest higher resistance to the damaging effects of the UV radiation because of both shielding and drying; it is widely known that UV damage produces pyrimidine dimers in nucleic acid and biochemical reactions involving bond formation typically require a solvent-like water.

Prototype Big Box UV chamber for pallets

A prototype Big Box UV sterilizer, a proprietary UV-C decontamination device, was acquired for virus inactivation testing. The outside dimensions were 2.74 m × 2.24 m × 2.4 m with an interior large enough to accommodate a recommended maximum load with dimensions of 1.21 m wide x 1.21 m long × 1.52 m tall. Maximum interior load was 1,134 kg. The interior was lined on five surfaces with a total of 320 T8 Hg bulbs, each measuring 0.9 m long and emitting 254 nm UV-C radiation. A double-stacked pallet mock-up of dimensions 1.02 m × 1.22 m × 1.64 m was placed within the UV chamber (Figure 9), centered from left to right, and positioned up against the rear backstop on the base of the chamber.

During testing, coupons were placed in Petri dishes on top of the pallet in five separate locations with lids removed prior to exposure. The UV chamber doors were closed, and the chamber was operated *via* a pre-programmed cycle set to run for 2 min followed by a 30 s exhaust. After UV exposure, the coupons were recovered, and the surviving virus was extracted and quantified. There was a single combined 2 min exposure test run for all coupons except for ABS plastic coupons, which were tested for 2 min on a separate test day. Room temperature extraction control samples were transported to and from the test location along with test coupons. Peak ozone generated was 0.36 ppm. Ozone was purged out of the chamber top for 30 s prior to opening the doors.

Results for the prototype Big Box UV sterilizer are shown in summary Tables 2, 3. A large double-stacked pallet mock-up was set inside the Big Box UV sterilizer. Coupons were then set on top of the plastic and cardboard mock-up for UV exposure, and the distance from virus-inoculated coupon to the nearest Hg bulbs on the chamber ceiling was 16.5 cm. The dosages varied

significantly at different locations in the box, resulting in a dosage range of 377–729 mJ cm⁻² for the test materials. Virus inactivation test results after UV treatment of 8.4 log₁₀ PFU of enveloped virus deposited per coupon (8.2 log₁₀ PFU for ABS plastic) showed a ≥5 log₁₀ PFU inactivation for SS304, polyurethane, and ABS plastic and a ≥3 log₁₀ PFU inactivation for NTC and cardboard. As for all other devices, the hardest, smoothest material (SS304) was most effectively treated while the most porous material (cardboard) was hardest to decontaminate.

Overall, the prototype Big Box chamber showed higher virus inactivation compared to almost all other devices, corresponding to the significantly higher UV dosage achieved with the large number of Hg bulbs in the chamber. The data highlight the overall limitations of UV technology to provide complete virus inactivation since virus sterilization was not achieved despite a large, powerful system featuring a total of 320 Philips T8 Hg bulbs.

Prototype fixed UV devices for room decontamination

Three prototype devices were also tested that were intended to be installed on the ceiling or wall to provide viral decontamination of the air. These devices followed the same general concept but differed slightly in the design and were tested in iterations that featured different UV radiation sources (Hg and KrCl bulbs). Test setup for these devices was largely similar to the previous devices with each test being carried out for five coupons and each inoculated from one of five independent viral preparations. Sterile control and extraction control coupons were also included. However, only one coupon material was tested for each device. Because the purpose of these devices is air decontamination, the specific test material employed here was not particularly important as long as the material was non-porous with the high extraction efficiency, and the materials provided no additional decontamination properties. SS304 was initially used for testing and was later replaced by quartz glass in one case, as it allows greater UV transmittance to maximize the surface area that would be exposed to UV and is similar to the way air particles would be exposed at all angles to direct or reflect UV. Testing virus-inoculated glass was a late decision during testing that increased the likelihood of UV penetration from multiple angles in order to prove that UV was able to kill the majority of 8 log₁₀ dried virus challenge. The glass tests also provided time and distance data point that might be used in future iterations of aerosol testing to calculate and predict airflow requirements for air decontamination. Tests were carried out for 5, 10, and 15 s for each device, though the distance from the UV source differed for each device as described later. For all experiments, the devices were

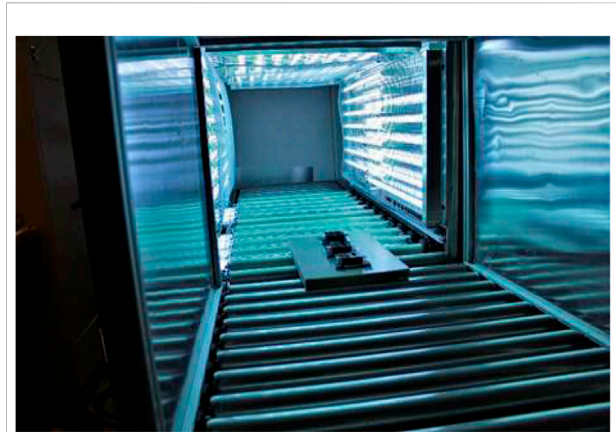


FIGURE 8
Dosimeters traveling down conveyor to determine exposure times for target UV dosages.

powered on for at least 30 min prior to testing to mitigate any start-up fluctuations in UV output.

Devices intended for air decontamination represent a challenge because methods to mimic respiratory enveloped virus for field testing (testing outside of laboratory containment), with a testing turnaround time of 2 weeks, have yet to be developed. While there are nebulization protocols for wet purified virus in laboratory testing, these methods have little practical relevance for field testing of environmentally relevant SARS-CoV-2 virus where the virus is protected by mucus (the surface of which primarily consists of carbohydrate), the infectious particles only consist of ≤0.001% virus, and the infectious 4 μm particles are dry, not wet (Hadi et al., 2020; Stadnytskyi et al., 2020). Laboratory testing of virus suspended in solution demonstrated that virus would not reproducibly survive shipping for field tests (Buhr et al., 2020). For the purposes of this work, the methods for field testing on virus-inoculated surfaces were maintained in order to comparatively screen and assess the effectiveness of the UV bulbs used in the different prototypes, particularly since there was so much variability in dosage and efficacy among different UV sources up to this point. This approach helped with iterative assessments and prototype improvements.

Prototype device A (Hg bulb and KrCl bulb iterations)

Prototype device A featured an internal UV source within an enclosed chamber. Fans controlled flow into the chamber where air was exposed to UV-C radiation and then exhausted through vents opposite from the fans. The first prototype contained two Philips TUV 15W/G15 T8 mercury bulbs, emitting 254 nm UV-C. Three fans were mounted in the device to provide airflow at

3,030 L min⁻¹ total through an effective inner volume of 24.64 L. This led to a residence time of 0.49 s that air would be exposed to UV radiation within the upper chamber. Exposures were at 5, 10, and 15 cm from the UV source.

The second iteration of device A replaced the dual Hg bulb with a single, custom KrCl excimer bulb from Far-UV Sterilray that emitted 222 nm UV-C, with the goal of developing a device with the good decontamination efficacy that also posed less of a hazard to personnel exposed to the UV source. The modified prototype A unit was determined to require approximately 5 min for the UV-C output to stabilize. The device was verified to emit a peak wavelength of 222 nm with a slight spike at 252 nm likely from the SiO₂ glass casing of the bulb (data not shown). The modified device A also included Teflon reflective surfaces to resist dirt build-up and provide reflectance of UV-C. High purity non-crystalline-fused silica glass plates, also called quartz glass, were added to channel airflow parallel to the UV-C source and increase the total contact time between contaminated air and UV-C. This increased the total UV dosage applied to air in the unit, thereby providing greater efficacy. The modified prototype device featured three fans providing 1,700 L min⁻¹ of airflow each into the unit. One fan always operated with the UV-C power switch. Two additional power switches were present for each additional fan; therefore, the device could operate at 1,700, 3,400, and 5,100 L min⁻¹ airflow. The effective interior volume was 24.33 L.

The efficacy of the UV source within the modified device A (KrCl bulb) was tested with the lid attached. Inoculated quartz glass test coupons were placed individually into a tray and slid inside the unit through slots cut in the frame. Slots were cut at set distances of 4, 10, and 20 cm from the center of the UV bulb. These distances were aligned to prominent design features in the box. The 4 cm test distance (4 cm from the center of the bulb or 2 cm from the edge of the bulb) aligned to an average distance from the bulb in the middle or second airflow channel. The 10 cm distance aligned to the outer channels just behind the quartz glass, and the 20 cm distance also aligned to the outer channels behind the glass at the furthest distance within the device where air would be exposed to UV-C.

Prototype device B (Hg bulb and KrCl bulb iterations)

Prototype device B featured a single UV-C source in an open-ended unit. Fans directed airflow into the underside of the unit, and air then exited the frame under and past the UV-C source and then out into the surrounding room air. As with device A, two iterations of the design were tested. The first iteration contained one Philips TUV PL-L 36W/4P Hg bulb. Device B was designed to be mounted on a wall and featured one fan to draw air upward from underneath the device and exhaust out the top and upper sides. It required a mounting height of 2.15 m in

order to ensure that no humans or pets are exposed to the UV-C coming out the sides of the device. Test exposures for this device were conducted at 5, 10 and 15 cm from the UV source. Coupons were placed in plastic Petri dishes with lids removed for exposures.

The second version of device B contained one KrCl excimer bulb, emitting 222 nm UV-C, the same bulb as in the second iteration of device A. With replacement of the 254 nm Hg bulb with 222 nm UV emission, it no longer had the strict requirement of a 2.15 m mounting distance, according to the prototype developer. However, 222 nm UV exposure was still a concern for Navy personnel. Device B contained limited Teflon as a reflective surface was placed near the bulb to direct and concentrate UV outward. Unlike device A, device B does not feature a closed compartment, where reflectivity with the Teflon can occur (substantially removing that potential for an increase in applied dosage). The device featured a recessed UV compartment between 10 and 15 cm deep with a cross-sectional area of 38.7 cm × 11.4 cm. The compartment was angled upward at approximately 45° from vertical to exhaust air and provide continuous UV exposure of ambient air. The average measured airflow at the compartment outlet was 2,237 L min⁻¹. Test exposures for this device were conducted at 5, 15, 30.5, 61, and 122 cm from the UV source. Coupons were placed in plastic Petri dishes with lids removed for exposures.

Prototype device C (Hg bulb type only)

Prototype device C followed a similar concept to device B but with a slightly different configuration and form factor. It was designed to be mounted on a wall and featured one Philips TUV 36W/G36 T8 Hg bulb and two internal fans, with the fans placed to draw air upward through the unit to exhaust out the top and upper sides. Like device B, it requires a mounting height of 2.15 m in order to ensure that no humans or pets are exposed to the UV-C coming out the upper sides of the device. Test exposures for this device were conducted at 5, 10, and 15 cm from the UV source. Coupons were placed in plastic Petri dishes with lids removed for exposures.

Mounted prototypes A, B (Hg bulb and KrCl bulb prototypes), and C (Hg bulb type only) efficacy

Efficacy results for the mounted prototypes A, B, and C are shown in Table 4 (log₁₀ reduction) and Table 5 (log₁₀ survival). Prototypes were tested at representative exposure distances, but the exposure times were much longer than expected for application in order to provide modeling data. Bio-efficacy testing on the original prototypes A, B, and C evaluated the performance of the UV source only. Testing on the modified



FIGURE 9

Prototype Big Box UV-C Chamber with a double-stacked pallet (top). Coupon placement was inside Petri plates on top of the pallet for testing (bottom).

prototypes A and B evaluated the internal improvements to the device. Thus, bio-efficacy data presented would be significantly less if realistic, shorter times were tested. For the original prototype A with the Hg bulbs, there was minimal \log_{10} reduction at different distances and times against virus-inoculated SS304. A modified prototype version with a greatly optimized internal configuration and a KrCl bulb was tested against virus-inoculated quartz glass. Time and cost restrictions prevented a test on virus-inoculated SS304. This modified prototype A unit showed a significant improvement over the original prototype. There were too many significant changes

between the first and second prototypes to isolate any single variable as the primary reason for the improved efficacy.

For the original prototype B with an Hg bulb, there was minimal \log_{10} reduction at different distances and times against virus-inoculated SS304. A modified prototype B with a KrCl bulb emitting 222 nm UV was tested. Test results showed worse efficacy results than the original prototype B. Overall, this device was the least effective of the wall-mounted prototypes, and it was not modified as extensively compared to the modified prototype A. The 222-nm KrCl bulb clearly did not improve the efficacy in this prototype.

Prototype C had an unfavorable design, and given its low efficacy, it was not pursued for modification.

Discussion

The aim of this research was to establish reference field test methods for UV decontamination of enveloped virus and to both assess and accelerate improvements in UV devices. $\Phi 6$ was selected as a BSL-1, enveloped RNA virus test indicator for both laboratory and field tests. $\Phi 6$ has been widely used as an enveloped virus surrogate (de Carvalho et al., 2017). It bears structural similarity to many other enveloped viruses including coronaviruses, suggesting that the $\Phi 6$ structure should be similarly susceptible to general decontaminants. The structural molecules of the virus are produced by host cells, with temperature sensitivity at around 40°C, further suggesting that $\Phi 6$ should be similarly susceptible to general decontaminants as animal coronaviruses. The capabilities for measuring the UV efficacy using both physics-based equipment and live, enveloped virus test indicators allowed standardized test measurements in both laboratory and field tests to directly compare the different UV devices.

Enveloped virus stability had been confirmed previously; purified virus was unstable, but unpurified virus was stable and could be stored dried onto coupons for at least 2 weeks prior to extraction (Buhr et al., 2020). The instability of enveloped virus in solution is a key difference compared to spore quantitation because spores are stable in non-nutrient aqueous solution at temperatures up to at least 65°C. Hence, wet spores can be stored at room temperature for many days alongside inoculated coupons (Buhr et al., 2012), whereas enveloped virus stored at ambient temperature was only stable after drying (Buhr et al., 2020). Furthermore, there was no $\Phi 6$ inactivation after unpurified virus was dried onto different surfaces and incubated for 10 days exposure to 26.7°C at 80% RH, and only 2.4 \log_{10} inactivation was seen after treatment at 70°C, 5% RH for 24 h (Buhr et al., 2020). More work will be needed to confirm that $\Phi 6$ and BSL-2/3 coronaviruses are stabilized similarly in the presence of carbohydrates and mucus, and after drying, but the first challenge is to generate sufficient BSL-2/3 coronavirus to match the titers (and statistical confidence) of the $\Phi 6$ tests. This goal has not yet been met. In addition, neither SARS-CoV-2 nor BSL-2 virus field testing is likely to happen with regularity.

The field testing in this manuscript is part of an iterative process of testing, test methods development, and UV analysis. These test methods serve as a baseline screening for military end users, military applications, and for military-relevant environments. To assess manufacturer claims of UV decontamination, different UV bulbs were directly tested with a live/dead enveloped virus assay at $>8 \log_{10}$ per test sample with five independent virus preparations per test material, and the

virus was dried >24 h prior to testing. Furthermore, $>50\%$ of inoculated virus was extracted from different control materials for up to 14 days after inoculation and showed to be “live” in a live/dead assay. These controls were needed to validate field test samples. In order to generate confidence and approve a device for end-user fielding, additional testing of aerosolized virus will need to be matured. Correlation tests among BSL-1, 2, and 3 enveloped viruses will need to be completed, and then tests will also need to be conducted inside buildings, ships, and aircrafts to adjust for variations in air movement and various power outages among all those locations. There will be no laboratory containment for field testing, so a live/dead assay using a BSL-1 organism will be needed for those tests. As described in the introduction, virus particles will need to be $>99.999\%$ non-volatile components, potentially including mucus for respiratory virus, where human airway mucus contains a high percentage of carbohydrates (Hadi et al., 2020). Here, the assay was simplified using $>99.999\%$ sucrose because sucrose is a carbohydrate with representative carbohydrate hydroxyls found on the surface of mucin, a glycoprotein critical to the function of mucus, and there were not sufficient data to define mucus and drying methods for coronavirus-relevant field testing during COVID-19. Furthermore, sucrose is a known stabilizer that has been historically used for virus purification, and it was empirically determined during $\Phi 6$ methods development to not inhibit the $\Phi 6$ plaque assay (Brakke 1951; 1967; Buhr et al., 2020). Sugars and amino acids also absorb some UV radiation (Uchiho et al., 2015) that can partially protect virus in the environment. This was a secondary benefit to increase confidence in the field test results since mucin is composed of sugars and amino acids.

This UV work was aimed at directly assessing claims that UV radiation would kill enveloped virus using a high confidence live/dead virus assay ($\geq 8 \log_{10}$ of dried virus with virus controls that were recoverable out to at least 2 weeks). Aerosol testing is another layer of testing that will be useful for UV decontamination screening. It is more complex because additional variables such as air movement need to be controlled, and high virus titers are needed in order to generate confidence that the data will represent environmental virus loads. Aerosol testing described in ASTM standard practice E2721-16 was a critical step forward for aerosol testing of wet-dispersed viruses, particularly influenza H1N1, and it described one potential artificial saliva recipe that can be added to virus samples (Heimbuch et al., 2011, Anonymous—ASTM International, 2016). The healthy saliva option contains 0.3% mucin and a total of $\sim 0.6\%$ non-volatiles, but the ASTM standard practice is flexible and not restricted to that option. This is important because a considerable amount of data describing mucus over the past decade were published after ASTM standard practice E2721-16. Saliva/oral fluids contain mucin glycoprotein, electrolytes, proteins, DNA, lipids, and host cell debris: remnants of dehydrated epithelial and white blood cells (Williams et al., 2006; Lai et al., 2009; Vejerano and Marr 2018; Hadi et al., 2020).

TABLE 4 Dosage and efficacy of room air-irradiating prototypes showing log₁₀ reduction data based on the average power from the bulb area, not the peaks. White (low decontamination) = Fail <2 log₁₀; yellow (sanitation) = Fail ≥2 log₁₀, <3 log₁₀; light blue (disinfection) = Pass ≥3 log₁₀; and dark blue (approaching virus sterilization) = Pass ≥6 log₁₀. N/A—dosage measurements had no meaning because of the broad-spectrum Xe source.

Name	Description	Dosage (mJ cm ⁻²)	Exposure distance (cm)	Exposure time (s)	Efficacy (log ₁₀ reduction after a >8 log ₁₀ challenge of live Φ6)	
					SS 304	Quartz glass
Ceiling mounted prototype A: original	Two Hg bulbs within an enclosed chamber and fans circulate air through unit 254 nm UV-C	18.6	5	5	0.9 ± 0.1	NA
		37.2		10	1.3 ± 0.1	NA
		55.8		15	1.7 ± 0.1	NA
		12.9	10	5	0.6 ± 0.1	NA
		25.7		10	1.0 ± 0.1	NA
		38.6		15	1.3 ± 0.1	NA
		10.6	15	5	0.5 ± 0.1	NA
		21.1		10	0.8 ± 0.1	NA
		31.7		15	1.1 ± 0.1	NA
Wall-mounted device A: modified	KrCl/excimer lamp within enclosed chamber and fans circulate air through unit 222 nm UV-C	15.2	4	5	NA	5.5 ± 0.6
		30.5		10	NA	6.4 ± 0.3
		45.8		15	NA	6.6 ± 0.7
		6.9	10	5	NA	2.2 ± 0.2
		13.7		10	NA	4.6 ± 0.7
		20.6		15	NA	6.7 ± 0.2
		3.4	20	5	NA	1.3 ± 0.1
		6.8		10	NA	2.4 ± 0.3
		10.2		15	NA	4.0 ± 0.6
Wall-mounted prototype B: original	Hg bulb within open sconce and fans circulate air through unit 254 nm UV-C	29.9	5	5	1.6 ± 0.1	NA
		59.8		10	2.5 ± 0.1	NA
		89.7		15	3.4 ± 0.1	NA
		15.8	10	5	1.1 ± 0.1	NA
		31.6		10	1.7 ± 0.1	NA
		47.4		15	2.3 ± 0.1	NA
		9.9	15	5	0.8 ± 0.1	NA
		19.7		10	1.3 ± 0.2	NA
		29.6		15	1.5 ± 0.1	NA
Wall-mounted prototype B: modified	KrCl/excimer lamp within open sconce and fans circulate air through unit 222 nm UV-C	15.6	5	5	0.5 ± 0.1	NA
		31.2		10	0.9 ± 0.2	NA
		46.8		15	1.2 ± 0.3	NA
		7.5	15	5	0.6 ± 0.2	NA
		15.0		10	0.5 ± 0.3	NA
		22.5		15	0.9 ± 0.1	NA
		2.8	30.5	5	0.1 ± 0.1	NA
		5.6		10	0.2 ± 0.1	NA
		8.4		15	0.2 ± 0.2	NA
		0.2	61	5	0.0 ± 0.2	NA
		0.3		10	0.0 ± 0.2	NA

(Continued on following page)

TABLE 4 (Continued) Dosage and efficacy of room air-irradiating prototypes showing \log_{10} reduction data based on the average power from the bulb area, not the peaks. White (low decontamination) = Fail $<2 \log_{10}$; yellow (sanitation) = Fail $\geq 2 \log_{10}$, $<3 \log_{10}$; light blue (disinfection) = Pass $\geq 3 \log_{10}$; and dark blue (approaching virus sterilization) = Pass $\geq 6 \log_{10}$. N/A—dosage measurements had no meaning because of the broad-spectrum Xe source.

Name	Description	Dosage (mJ cm^{-2})	Exposure distance (cm)	Exposure time (s)	Efficacy (\log_{10} reduction after a $>8 \log_{10}$ challenge of live $\Phi 6$)	
					SS 304	Quartz glass
		0.5		15	0.1 ± 0.1	NA
		0.1	71	5	0.0 ± 0.1	NA
		0.2		10	0.0 ± 0.1	NA
		0.3		15	0.0 ± 0.1	NA
Wall-mounted prototype C	Hg bulb within open scone and fans circulate air through unit 254 nm UV-C	16.6	5	5	0.9 ± 0.2	NA
		33.2		10	1.6 ± 0.0	NA
		49.8		15	2.2 ± 0.2	NA
		9.1	10	5	0.7 ± 0.1	NA
		18.2		10	0.9 ± 0.1	NA
		27.3		15	1.3 ± 0.1	NA
		6.4	15	5	0.5 ± 0.1	NA
		12.8		10	0.8 ± 0.0	NA
		19.2		15	1.2 ± 0.1	NA

Mucin glycoproteins are critical to the function of mucus (Lai et al., 2009), and there are over 20 different types of mucin in humans (Corfield 2015). Similar to sucrose, hydroxyl groups on mucin glycans control water activity (Znamenskaya et al., 2012). Unlike sucrose, the glycan subunits on different mucins are variable, which creates variability in water activity as it pertains to mucin resuspension from dried, commercial sources, and in mucin gel formation (Znamenskaya et al., 2012). Hence, selection of sucrose for field testing during COVID-19 was a simple, homogenous replacement that was easy to standardize for the live/dead screening tests conducted early during COVID-19. Furthermore, critical characterization data needed for accurate and relevant SARS-CoV-2 inactivation testing, such as COVID-19 mucus characterization (Kratochvil et al., 2022), are beginning to be published only now.

Commercially, two common animal mucins are readily available and frequently used: porcine gastric mucin (PGM) and bovine submaxillary mucin (BSM). PGM is sourced from intestinal epithelium and is desired in experiments due to its sialic acid content that best matches respiratory mucins. BSM is sourced from submaxillary glands in the floor of a cow's mouth. Mucin is a major element of saliva, and another component of saliva than can interact with mucin is a lung surfactant, which is made up of about 90% phospholipids and 10% proteins (Bredberg et al., 2012). The most abundant and active phospholipid in respiratory droplets is

dipalmitoylphosphatidylcholine (DPPC) (Niazi et al., 2021). A DPPC saliva recipe (0.9%, sodium chloride, 0.3% porcine gastric mucin, and 0.05% DPPC) was mixed with $\Phi 6$, as an enveloped virus surrogate for H1N1, and DPPC protected the mucin to prevent gel formation (Vejerano and Marr 2018). Thus, saliva phospholipids are another potentially important ingredient that might be added to mucus recipes for future iterations of decontamination testing.

The impact of drying on virus stability was a similarly important topic as it is known that enveloped viruses are stabilized by drying (Cox and Wathes, 1995), and SARS-CoV-2 virus has been shown to survive for up to 4 weeks after drying on materials (Riddell et al., 2020). Drying for >24 h was a practical requirement for field testing in this work since samples were routinely shipped to and from test sites. Future aerosol field tests would likely require virus release and monitoring over time, which are beyond the current scope of existing test methods. Defining a final quantity of non-volatiles to generate a standardized mucus solution to mix with enveloped virus is further complicated by the prospect that respiratory disease-afflicted individuals may produce a thicker and/or dryer mucus during different stages of illness as compared to healthy persons (Vejerano and Marr 2018; Kratochvil et al., 2022). Coronavirus particle measurements in 2020 indicated that 12–21 μm speech particles would dry to 4 μm particles in seconds and smaller particles <1 μm in size have such a small

TABLE 5 Dosage and efficacy of room air-irradiating prototypes showing log₁₀ survival data based on the average power from the bulb area, not the peaks. White (low decontamination) = Fail <2 log₁₀; yellow (sanitation) = Fail ≥2 log₁₀, <3 log₁₀; light blue (disinfection) = Pass ≥3 log₁₀; and dark blue (approaching virus sterilization) = Pass ≥6 log₁₀. N/A—dosage measurements had no meaning because of the broad-spectrum Xe source.

Name	Description	Dosage (mJ cm ⁻²)	Exposure distance (cm)	Exposure time (s)	Log ₁₀ survival after a >8 log ₁₀ challenge of live Φ6		
					Inoculum	SS304	Quartz glass
Ceiling-mounted prototype A: original	Two Hg bulbs within enclosed chamber and fans circulate air through unit 254 nm UV-C	18.6	5	5	8.2 ± 0.0	7.3 ± 0.3	NA
		37.2		10		6.9 ± 0.1	NA
		55.8		15		6.5 ± 0.2	NA
		12.9	10	5	7.6 ± 0.2	7.6 ± 0.2	NA
		25.7		10		7.2 ± 0.3	NA
		38.6		15		7.0 ± 0.1	NA
		10.6	15	5	7.8 ± 0.1	7.8 ± 0.1	NA
		21.1		10		7.4 ± 0.3	NA
		31.7		15		7.1 ± 0.2	NA
		Wall-mounted prototype A: modified	KrCl/excimer lamp within enclosed chamber and fans circulate air through unit 222 nm UV-C	15.2	4	5	8.2 ± 0.1
30.5	10			NA		1.8 ± 0.7	
45.8	15			NA		1.6 ± 1.6	
6.9	10			5	NA	6.0 ± 0.5	6.0 ± 0.5
13.7				10		3.5 ± 1.5	3.5 ± 1.5
20.6				15		1.4 ± 0.4	1.4 ± 0.4
3.4	20			5	NA	6.8 ± 0.3	6.8 ± 0.3
6.8				10		5.7 ± 0.7	5.7 ± 0.7
10.2				15		4.1 ± 1.3	4.1 ± 1.3
Wall-mounted prototype B: original	Hg bulb within open sconce and fans circulate air through unit 254 nm UV-C			29.9	5	5	8.2 ± 0.0
		59.8	10	5.7 ± 0.2		NA	
		89.7	15	4.8 ± 0.3		NA	
		15.8	10	5	7.1 ± 0.2	7.1 ± 0.2	NA
		31.6		10		6.5 ± 0.2	NA
		47.4		15		5.9 ± 0.3	NA
		9.9	15	5	7.5 ± 0.2	7.5 ± 0.2	NA
		19.7		10		6.9 ± 0.4	NA
		29.6		15		6.7 ± 0.2	NA
		Wall-mounted prototype B: modified	KrCl/excimer lamp within open sconce and fans circulate air through unit 222 nm UV-C	15.6	5	5	8.1 ± 0.3
31.2	10			7.2 ± 0.4		NA	
46.8	15			6.9 ± 0.6		NA	
7.5	15			5	7.6 ± 0.2	7.6 ± 0.2	NA
15.0				10		7.6 ± 0.6	NA
22.5				15		7.2 ± 0.1	NA
2.8	30.5			5	8.1 ± 0.1	8.1 ± 0.1	NA
5.6				10		7.9 ± 0.2	NA
8.4				15		7.9 ± 0.2	NA
0.2	61			5	8.1 ± 0.2	8.1 ± 0.2	NA
0.3		10	8.1 ± 0.2	NA			

(Continued on following page)

TABLE 5 (Continued) Dosage and efficacy of room air-irradiating prototypes showing \log_{10} survival data based on the average power from the bulb area, not the peaks. White (low decontamination) = Fail $<2 \log_{10}$; yellow (sanitation) = Fail $\geq 2 \log_{10}$, $<3 \log_{10}$; light blue (disinfection) = Pass $\geq 3 \log_{10}$; and dark blue (approaching virus sterilization) = Pass $\geq 6 \log_{10}$. N/A—dosage measurements had no meaning because of the broad-spectrum Xe source.

Name	Description	Dosage (mJ cm^{-2})	Exposure distance (cm)	Exposure time (s)	Log ₁₀ survival after a $>8 \log_{10}$ challenge of live $\Phi 6$		
					Inoculum	SS304	Quartz glass
		0.5		15		8.0 ± 0.1	NA
		0.1	71	5		8.1 ± 0.1	NA
		0.2		10		8.1 ± 0.1	NA
		0.3		15		8.1 ± 0.2	NA
Wall-mounted prototype C	Hg bulb within open sconce and fans circulate air through unit 254 nm UV-C	16.6	5	5	8.2 ± 0.0	7.4 ± 0.3	NA
		33.2		10		6.7 ± 0.1	NA
		49.8		15		6.1 ± 0.3	NA
		9.1	10	5		7.5 ± 0.2	NA
		18.2		10		7.3 ± 0.2	NA
		27.3		15		6.9 ± 0.2	NA
		6.4	15	5		7.7 ± 0.1	NA
		12.8		10		7.4 ± 0.1	NA
		19.2		15		7.1 ± 0.1	NA

probability of containing virus that such a size is likely negligible for infection (Stadnytskyi et al., 2020). A volume/volume calculation indicates that the 12–21 μm particles would contain 0.8–3.7% non-volatiles to generate $\sim 4 \mu\text{m}$ dried particles. Assuming a worst case scenario where the highest level of non-volatiles is protecting enveloped virus, then a mucus recipe with 3.7% non-volatiles contains about 3–6x more non-volatiles compared to existing mucus recipes with 0.6–1.25% total non-volatiles (Aps and Martens, 2005; Heimbuch et al., 2011; ASTM 2016; Vejerano and Marr 2018). COVID-19 mucus characterization was recently published showing a mean load of $\sim 4.7\%$ solids and significantly higher amounts of mucin glycoprotein and DNA compared to healthy samples (Kratochvil et al., 2022). The characterization data for COVID-19 mucus non-volatile ingredients were not available when this UV decontamination work started, but these data will impact future iterations of testing.

A $\geq 8 \log_{10}$ challenge level was initially set for $\Phi 6$ testing because measurements with high concentrations of microbes greatly increase the confidence in inactivation and mitigate the risk of incomplete decontamination (Hamilton et al., 2013). Furthermore, coronavirus nasal swabs showed $>8 \log_{10}$ virus per swab as calculated using a PCR assay (Leung et al., 2020; Stadnytskyi et al., 2020), and a recent human infection study showed $8.9 \log_{10}$ genomic copies ml^{-1} from nasal samples 5 days after infection (Killingley et al., 2022). The limitation of genomic

sampling is that it does not equate to infectious particles. However, an individual highly infected with SARS-CoV-2 can emit $>8 \log_{10}$ virus particles in a 24 h period (Stadnytskyi et al., 2020). Extrapolation of that data indicates that multiple personnel within confined spaces, limited ventilation, and low humidity may generate considerably $>8 \log_{10}$ of infectious virus at any given point in time and is a critical consideration in both military and transportation applications. The infectious particle data further justify the need for $\geq 8 \log_{10}$ challenge regardless of whether the virus is aerosolized or on surfaces.

UV radiation does not fall under the United States Environmental Protection Agency (EPA) jurisdiction for disinfection claims since it is not classified as a chemical disinfectant. Nonetheless, for this study that began in 2020, the inactivation goal was reduced from $\geq 7 \log_{10}$ to $\geq 3 \log_{10}$ inactivation during the COVID-19 pandemic to match the EPA N-list for decontaminants. This was initially helpful because inactivation numbers for sanitation, disinfection, and sterilization (Rutala and APIC Committee, 1996) could be used for assessments of decontaminants including UV. However, the $3 \log_{10}$ kill threshold is now in question because a very recent human infection study showed that only 10 TCID₅₀ of wild-type SARS-CoV-2 (equivalent to ~ 7 PFU) was needed to infect $>50\%$ of unvaccinated humans in a 36-volunteer group, with no prior infection (Killingley et al., 2022). This human infection study validates the original quantitative objective to show

enveloped virus inactivation of $\geq 7 \log_{10}$ out of a $\geq 8 \log_{10}$ challenge in order to increase decontamination confidence. These high kill objectives/requirements are important to validate decontamination claims for respiratory pathogens, which spread rapidly and continuously through air and likely also through surface transfer. The wide variability in virus preparation and test methods and the associated results published during COVID-19 has decreased end-user confidence levels for evaluating decontaminants (Hadi et al., 2020). The limitation of direct SARS-CoV-2 virus testing is the lack of statistically significant test data with multiple independent preparations of virus at high virus titers ($>10 \log_{10}$ of virus ml^{-1} of culture medium at the time of virus harvest and without virus concentration or purification). These quantitative requirements need to be addressed in order to generate end-user confidence that data can be reproduced (statistical accuracy) and that virus titers can match the virus stabilization and quantities that may be encountered in the environment.

This background data indicate that detailed methods for mucus and aerosol testing of respiratory coronavirus will need to be defined, characterized, and developed for future iterations of decontamination testing. These should also include correlation testing among biosafety level 1, 2, and 3 enveloped viruses. Data from methods with increasingly higher confidence will improve the likelihood of end-user acceptance of UV technologies. The work here showed that enveloped virus could be field tested at $>8 \log_{10}$ of stabilized enveloped virus using multiple preparations of virus and a live/dead assay. The quantitation could be reproduced and field tested with a 2-weeks data turnaround to provide an initial UV screening/selection. The UV test results here also showed that high UV dosages are needed to inactivate enveloped virus protected by environmental debris, and porous materials are difficult to decontaminate, particularly in comparison to purified virus alone. These limitations of UV are well-documented by regulatory agencies, and they also apply to SARS-CoV-2 (United States Food and Drug Administration 2021a; United States Environmental Protection Agency 2021). Nonetheless, the UV efficacy was measurable and very high dosages were effective even on relatively porous materials like cardboard. It is unlikely that UV would be useful for highly porous fabrics, which are used to make bags, carpeting, and clothing, and those were not tested. In contrast, hot, humid air inactivates debris-laden microbes with similar kinetics regardless of material porosity (Buhr et al., 2012; 2015; 2016; 2020). This is a hallmark difference between highly penetrative decontaminants and a surface decontaminant like UV.

The antiviral efficacy among the different UV devices ranged from no decontamination up to nearly achieving enveloped virus sterilization. Enormous variability in dosage and efficacy was measured within and among the different devices. The prototype medium conveyer generated the highest virus inactivation per dosage. Inoculated coupons were exposed to UV-C on three

sides since the coupons were set on a flat surface during exposure in the conveyer. The big UV box also generated high levels of virus inactivation, but the medium conveyer had highest efficacy dose^{-1} . In contrast the handheld devices, pulsed Xenon devices, LEM, and the original prototypes A, B, and C, and modified prototype B were all evaluated with a UV source emitted from predominantly one direction with slightly varying angles of exposure. The increased angles of exposure in the conveyer and big box likely improved UV-C penetration. Hence, the unique geometry, design, and electronics of each device impacted the effectiveness above and beyond the wavelength and dosage.

The variability seen among the various tested devices strongly indicates that all UV devices need to be measured for both UV dosage and for antiviral efficacy before they are incorporated into decontamination protocols. The efficacy of a pulsed Xe bulb was measurable at close distances, but they were significantly lower than Hg bulbs. Pulsed Xe devices do have some practical advantages such as requiring minimal warm-up time and no Hg toxicity. LEDs have the lowest hazard and lowest variability in UV output. However, the availability of UV LEDs has been limited, and UV dosages can also be limiting depending on the manufacturer, model, and the electronics and overall design of any given device. Longer wavelength UV (272 nm) showed the best efficacy in handheld devices, and 272 nm is more penetrating than short wavelengths. The 222-nm KrCl sources showed measurable efficacy in conjunction with proprietary prototype advancements. Additional testing with $>8 \log_{10}$ debris-laden virus is needed because the 222-nm KrCl testing was limited due to time and cost constraints.

Finally, decontamination with UV comes with tradeoffs that affect the decision of the end user. The time of exposure needed to generate the efficacy needs to be assessed by end users because long exposure times will limit the utility of UV, especially for handheld and air decontamination devices. Use of handheld UV devices is also very hard to standardize, which increases safety risks for end users (United States Food and Drug Administration 2021b). Another tradeoff to be assessed by end users is the need for cleaning and maintenance of UV devices to remove dirt and debris that accumulates on the radiation sources and/or to change radiation sources. Devices and methods to monitor UV dosage over time are needed to assist in maintenance, a particularly important subject that is rarely addressed. Additional tradeoffs are ozone generation, which reached toxic levels up to 3.6 times higher than OSHA limits for some devices (Claus 2021), and operation times. Hg bulbs, in particular, require warm-up times in order to reach a steady state. In general, Hg bulbs generate a maximum intensity quickly, and then the intensities were stabilized at a lower level after a warm-up period. The Hg devices which have performed better had only this initial dose been tested, but that data would not translate to practical application because it will be hard to standardize turn-on times for end users,

especially for handhelds. Last, the end user needs an understanding of the organism(s) to be killed, how it is stabilized in the environment, and the impact of test methods on results, as these factors will impact confidence in any application. Assessment of these tradeoffs will facilitate practical application of UV decontamination. UV has potential for augmenting current practices for limiting the spread of enveloped virus, but UV cannot and should not replace normal cleaning and hygienic practices or air filtration and ventilation. Equipment breakdowns/failures, electrical outages, and maintenance shortcomings are common, normal, and realistic. Hence, coronavirus test methods need to significantly improve in order to approximate realistic environmental conditions with debris-laden, dried, high titer virus and increase UV test confidence. As test standards, UV field validation methods, and UV sources improve, UV might become a more viable option for augmenting decontamination in some applications. Multiple layers of testing, including field validation testing such as that described herein, will be needed because of the extraordinary variability of UV output from different devices. In addition, methods to continuously monitor UV output and maintenance and cleaning guidelines are critical areas that need to be addressed.

Data availability statement

The original contributions presented in the study are included in the article/Supplementary Materials; further inquiries can be directed to the corresponding author.

Author contributions

TB was the principal investigator and primary author. All authors from the Naval Surface Warfare Center-Dahlgren participated in virus test preparation, testing, data acquisition/organization/assembly, and writing. All authors from the Naval Research Laboratory participated in ultraviolet light dosage testing, analysis and writing.

References

- Aps, J. K. M., and Martens, L. C. (2005). Review: The physiology of saliva and transfer of drugs into saliva. *Forensic Sci. Int.* 150 (2-3), 119–131. doi:10.1016/j.forsciint.2004.10.026
- ASTM International (formerly the American Society for Testing and Materials) (2016). *Evaluation of effectiveness of decontamination procedures for surfaces when challenged with droplets containing human pathogenic viruses*. ASTM Standard Practice E2721-16.
- ASTM International (formerly the American Society for Testing and Materials) (2020). Guidance on SARS-CoV-2 surrogate selection. Available at: <https://www.astm.org/COVID-19/> (Accessed on September 15, 2021).

Funding

This work was supported through funding and program support provided by Naval Sea Systems Command, Defense Innovation Unit, Naval Medical Research Center Naval Advanced Medical Development (NMRC-NAMD), the Defense Threat Reduction Agency (DTRA), and Hazard Mitigation Capability Area (BA2 and 3 funds, Project Number CB10141).

Acknowledgments

The authors thank Rich Wiersteiner, Jon Cofield, Heather Ichord, Janet Weir, Glenn Lawson, Chuck Bass, James Noah, John Aaron Miller, and Joe Schumer for support. They thank Jason A. Fallen, Joseph Hunt, Carlos Murillo, Kira Baugh, and Julie Caruana for outstanding technical support and/or assistance with editing the manuscript. This manuscript was approved for public release on 1/27/2022 as #6156; NSWCDD PN-22-00021 and 8/1/2022 as #6232; NSWCDD PN-22-00131 and will be released as a pre-print at bioRxiv (Buhr et al.).

Conflict of interest

The authors declare that the research was conducted in the absence of any commercial or financial relationships that could be construed as a potential conflict of interest.

Publisher's note

All claims expressed in this article are solely those of the authors and do not necessarily represent those of their affiliated organizations, or those of the publisher, the editors, and the reviewers. Any product that may be evaluated in this article, or claim that may be made by its manufacturer, is not guaranteed or endorsed by the publisher.

ASTM International (formerly the American Society for Testing and Materials) (2018b). *Standard practice for evaluating efficacy of vaporous decontaminants against Bacillus spores contained within 0.2µm filter-capped tubes*. ASTM Standard Practice E3092-18.

ASTM International (formerly the American Society for Testing and Materials) (2018a). *Standard practice for evaluating static and tidal chemical decontaminants against Bacillus spores using centrifugal filtration tubes*. ASTM Standard Practice E3178-18.

- Bibby, K., Casson, L. W., Stachler, E., and Haas, C. N. (2015). Ebola virus persistence in the environment: State of the knowledge and research needs. *Environ. Sci. Technol. Lett.* 2, 2–6. doi:10.1021/ez5003715
- Brakke, M. K. (1951). Density gradient centrifugation: A new separation technique. *J. Am. Chem. Soc.* 73, 1847–1848.
- Brakke, M. K. (1967). "Density-gradient centrifugation," In *Methods in virology*. Editors K. Maramorosch and H. Koprowski (New York: Academic Press), 2, 93–118.
- Bredberg, A., Gobom, J., Almstrand, A., Larsson, P., Blennow, K., Olin, A., et al. (2012). Exhaled endogenous particles contain lung proteins. *Clin. Chem.* 58 (2), 431–440.
- Brown, J. S., Gordon, T., Price, O., and Asgharian, B. (2013). Thoracic and respirable particle definitions for human health risk assessment. *Part. Fibre Toxicol.* 10, 1–12.
- Buhr, T. L., Young, A. A., Borgers-Klonkowski, E., Kennihan, N. L., Barnette, H. K., Minter, Z. A., et al. (2020). Hot, humid air decontamination of aircraft confirmed that high temperature and high humidity are critical for inactivation of infectious, enveloped ribonucleic acid (RNA) virus. *Front. Bioeng. Biotechnol.* 8, 592621. doi:10.3389/fbioe.2020.592621
- Buhr, T. L., Young, A. A., Minter, Z. A., and Wells, C. M. (2012). Test method development to evaluate hot, humid air decontamination of materials contaminated with *Bacillus anthracis* ΔSterne and *B. thuringiensis* Al Hakam spores. *J. Appl. Microbiol.* 113, 1037–1051. doi:10.1111/j.1365-2672.2012.05423.x
- Buhr, T., Young, A. A., Barnette, H., Minter, Z. A., Kennihan, N., McPherson, D. C., et al. (2015). Test methods and response surface models for hot, humid air decontamination of materials contaminated with dirty spores of *Bacillus anthracis* ΔSterne and *B. thuringiensis* Al Hakam. *J. Appl. Microbiol.* 119, 1263–1277.
- Buhr, T., Young, A. A., Johnson, C. A., Minter, Z., and Wells, C. (2014). Decontamination of materials contaminated with *Francisella philomiragia* or MS2 bacteriophage using PES-Solid, a solid source of peracetic acid. *J. Appl. Microbiol.* 117, 397–404. doi:10.1111/jam.12540
- Buhr, T., Young, A., Bensman, M., Minter, Z., Kennihan, N., Johnson, C., et al. (2016). Hot, humid air decontamination of a C-130 aircraft contaminated with spores of two acrySTALLIFEROUS *Bacillus thuringiensis* strains, surrogates for *Bacillus anthracis*. *J. Appl. Microbiol.* 120, 1074–1084. doi:10.1111/jam.13055
- Chan, K. H., Malik Peiris, J. S., Lam, S. Y., Poon, L. L. M., Yuen, K. Y., and Seto, W. H. (2011). The effects of temperature and relative humidity on the viability of the SARS coronavirus. *Adv. Virol.* 7. Article ID 734690. doi:10.1155/2011/734690
- Claus, H. (2021). Ozone generation by ultraviolet lamps. *Photochem Photobiol.* 97, 471–476.
- Corfield, A. P. (2015). Mucins: A biologically relevant glycan barrier in mucosal protection. *Biochim. Biophys. Acta* 1850 (1), 236–252. doi:10.1016/j.bbagen.2014.05.003
- Cox, C. S., and Wathes, C. M. (1995). *Bioaerosols handbook*. 1st ed. (Boca Raton: CRC Press), 656. doi:10.1201/9781003070023
- de Carvalho, N. A., Stachler, E. N., Cimabue, N., and Bibby, K. (2017). Evaluation of Phi6 persistence and suitability as an enveloped virus surrogate. *Environ. Sci. Technol.* 51 (15), 8692–8700. doi:10.1021/acs.est.7b01296
- Fedorenko, A., Grinberg, M., Orevi, T., and Kashtan, N. (2020). Survival of the enveloped bacteriophage Phi6 (a surrogate for SARS-CoV-2) in evaporated saliva microdroplets deposited on glass surfaces. *Sci. Rep.* 10, 22419. doi:10.1038/s41598-020-79625-z
- Fenn, E. A. (2001). *Pox americana: The great smallpox epidemic of 1775–82*. New York: Hill and Wang.
- Gallandat, K., and Lantagne, D. (2017). Selection of a Biosafety Level 1 (BSL-1) surrogate to evaluate surface disinfection efficacy in Ebola outbreaks: Comparison of four bacteriophages. *PLoS ONE* 12 (5). doi:10.1371/journal.pone.0177943
- Goldsmith, C. S., Tatti, K. M., Ksiazek, T. G., Rollin, P. E., Comer, J. A., Lee, W. W., et al. (2004). Ultrastructural characterization of SARS coronavirus. *Emerg. Infect. Dis.* 10 (2), 320–326. doi:10.3201/eid1002.030913
- Greiff, D., Blumenthal, H., Chiga, M., and Pinkerton, H. (1954). The effects on biologic materials of freezing and drying by vacuum sublimation II. Effect on influenza virus. *J. Exptl Med.* 100 (1), 89–101.
- Greiff, D., and Rightel, W. (1966). In *Freezing and freeze-drying of viruses*. *Cryobiology*. Editor H. T. Meryman (New York, USA: Academic Press), 697–728.
- Hadi, J., Dunowska, M., Wu, S., and Brightwell, G. (2020). Control measures for SARS-CoV-2: A review on light-based inactivation of single-stranded RNA viruses. *Pathogens* 9, 737–767. doi:10.3390/pathogens9090737
- Hamilton, M., Hamilton, G., Goeres, D., and Parker, A. (2013). Guidelines for the statistical analysis of a collaborative study of a laboratory disinfectant product performance test method. *JAOAC Int.* 96 (5), 1138–1151. doi:10.5740/jaoacint.12-217
- Heimbuch, B. K., Wallace, W. H., Kinney, K., Lumley, A. E., Wu, C. Y., Woo, M. H., et al. (2011). A pandemic influenza preparedness study: Use of energetic methods to decontaminate filtering facepiece respirators contaminated with H1N1 aerosols and droplets. *Am. J. Infect. Control* 39, e1–e9.
- Hendley, J. O., Wenzel, R. P., and Gwaltney, J. M., Jr. (1973). Transmission of rhinovirus colds by self-inoculation. *N. Engl. J. Med.* 288, 1361–1364.
- Heßling, M., Hönes, K., Vatter, P., and Lingenfelder, C. (2020). Ultraviolet irradiation doses for coronavirus inactivation – review and analysis of coronavirus photoinactivation studies. *GMS Hyg. Infect. Control* 15, 2196–5226. doi:10.3205/2Fdgkh000343
- Hofer, S., Hofstätter, N., Duschl, A., and Himly, M. (2021). SARS-CoV-2-Laden respiratory aerosol deposition in the lung alveolar-interstitial region is a potential risk factor for severe disease: A modeling study. *J. Pers. Med.* 11, 431. doi:10.3390/jpm11050431
- Killingley, B., Mann, A., Kalinova, M., Boyers, A., Goonawardane, N., Zhou, J., et al. (2022). Safety, tolerability and viral kinetics during SARS-CoV-2 human challenge. *Res. Square pre-print*, 1–27. doi:10.21203/rs.rs-1121993/v1
- Kratovichil, M. J., Kaber, G., Demirdjian, S., Cai, P. C., Burgener, E. B., Nagy, N., Barlow, G. L., Popescu, M., Nicolls, M. R., Ozawa, M. G., Regula, D. P., Pacheco-Navarro, A. E., Yang, S., de Jesus Perez, V. A., Karmouty-Quintana, H., Peters, A. M., Zhao, B., Buja, M. L., Johnson, P. Y., Vernon, R. B., Wight, T. N., Milla, C. E., Rogers, A. J., Spakowitz, A. J., Heilshorn, S. C., and Bollyky, P. L. Stanford COVID-19 Biobank Study Group (2022). Biochemical, biophysical, and immunological characterization of respiratory secretions in severe SARS-CoV-2 infections. *JCI Insight* 7 (12), e152629. doi:10.1172/jci.insight.152629
- Lai, S. K., Wang, Y., Wirtz, D., and Hanes, J. (2009). Micro- and macro-rheology of mucus. *Adv. Drug Deliv. Rev.* 61 (2), 86–100. doi:10.1016/j.addr.2008.09.012
- Leung, N. H. L., Chu, D. K. W., Shiu, E. Y. C., Chan, K.-H., McDevitt, J. J., Hau, B. J. P., et al. (2020). Respiratory virus shedding in exhaled breath and efficacy of face masks. *Nat. Med.* 26, 676–680. doi:10.1038/s41591-020-0843-2
- Malenovska, H. (2014). The influence of stabilizers and rates of freezing on preserving of structurally different animal viruses during lyophilization and subsequent storage. *J. Appl. Microbiol.* 117, 1810–1819. doi:10.1111/jam.12654
- Masters, P. S. (2006). The molecular biology of coronaviruses. *Adv. Virus Res.* 66, 193–292. doi:10.1016/S0065-3527(06)66005-3
- McDonnell, G., and Burke, P. (2011). Disinfection: Is it time to reconsider spaulding? *J. Hosp. Inf.* 78, 163–170. doi:10.1016/j.jhin.2011.05.00210.1016/j.jhin.2011.05.002
- Memarzadeh, F. (2021). A review of recent evidence for utilizing ultraviolet irradiation technology to disinfect both indoor air and surfaces. *Appl. Biosaf.* 26 (1), 52–56. doi:10.1089/apb.20.0056
- Mindich, L. (2004). Packaging, replication and recombination of the segmented genomes of bacteriophage Φ6 and its relatives. *Virus Res.* 101, 83–92. doi:10.1016/j.virus.2003.12.008
- Niazi, S., GrothSpann, R. K., and Johnson, G. R. (2021). The role of respiratory droplet physicochemistry in limiting and promoting the airborne transmission of human coronaviruses: A critical review. *Environ. Pollut.* 2021, 276.
- Raiszadeh, M., and Adeli, B. (2020). A critical review on ultraviolet disinfection systems against COVID-19 outbreak: Applicability, validation, and safety considerations. *ACS Photonics* 7 (11), 2941–2951. doi:10.1021/acsp Photonics.0c01245
- Riddell, S., Goldie, S., Hill, A., Eagles, D., and Drew, T. W. (2020). The effect of temperature on persistence of SARS-CoV-2 on common surfaces. *Virol. J.* 17 (1), 145. doi:10.1186/s12985-020-01418-7
- Rutala, W. A. APIC Committee (1996). APIC Guideline for selection and use of disinfectants. *Am. J. Infect. Cont.* 24, 313–342. doi:10.1016/S0196-6553(96)90066-8
- Stadnytskyi, V., Bax, C. E., Bax, A., and Anfinrud, P. (2020). The airborne lifetime of small speech droplets and their potential importance in SARS-CoV-2 transmission. *Proc. Natl. Acad. Sci.* 117 (2), 11875–11877. doi:10.1073/pnas.2006874117
- Tseng, C. C., and Li, C. S. (2005). Inactivation of virus-containing aerosols by ultraviolet germicidal irradiation. *Aerosol Sci. Technol.* 39, 1136–1142. doi:10.1080/2F15459620701329012
- Uchiho, Y., Goto, Y., Kamahori, M., Aota, T., Moriasaki, A., Hosen, Y., et al. (2015). Far-ultraviolet absorbance detection of sugars and peptides by high-performance liquid chromatography. *J. Chromatogr.* 1424, 86–91. doi:10.1016/j.chroma.2015.11.006
- United States Environmental Protection Agency (2021). Disinfecting surfaces with UV light to reduce exposure to SARS-CoV-2. Available at: <https://www.epa.gov/covid19->

research/disinfecting-surfaces-uv-light-reduce-exposure-sars-cov-2 (Accessed on September 15, 2021).

United States Food and Drug Administration (2021b). Risk of exposure to unsafe levels of radiation with safe-T-lite UV WAND: FDA safety communication. Available at: <https://www.fda.gov/medical-devices/safety-communications/risk-exposure-unsafe-levels-radiation-safe-t-lite-uv-wand-fda-safety-communication> (Accessed on July 20, 2022).

United States Food and Drug Administration (2021a). *UV lights and lamps: Ultraviolet-C radiation, disinfection, and coronavirus*. Available at: <https://www.fda.gov/medical-devices/coronavirus-covid-19-and-medical-devices/uv-lights-and-lamps-ultraviolet-c-radiation-disinfection-and-coronavirus> (Accessed on September 15, 2021).

van Doremalen, N., Bushmaker, T., and Munster, V. J. (2013). Stability of Middle East respiratory syndrome coronavirus (MERS-CoV) under different environmental conditions. *Euro Surveill.* 18 (38), 20590. doi:10.2807/1560-7917.ES2013.18.38.20590

Van Etten, J., Lane, L., Gonzalez, C., Partridge, J., and Vidaver, A. (1976). Comparative properties of bacteriophage phi6 and phi6 nucleocapsid. *J. Virol.* 18 (2), 652, 658).

Vejerano, E. P., and Marr, L. C. (2018). Physico-chemical characteristics of evaporating respiratory fluid droplets. *J. R. Soc. Interface* 15, 20170939. doi:10.1098/rsif.2017.0939

Vidaver, A. K., Roski, R. K., and Van Etten, J. L. (1973). Bacteriophage phi6: A lipid-containing virus of *Pseudomonas phaseolicola*. *J. Virol.* 11 (5), 799–805.

Weber, T. P., and Stilianakis, K. I. (2008). Inactivation of influenza A viruses in the environment and modes of transmission: A critical review. *J. Inf.* 57, 361–373. doi:10.1016/j.jinf.2008.08.013

Wiggington, K. R., Pecson, B. M., Sigstam, T., Bosshard, F., and Kohn, T. (2012). Virus inactivation mechanisms: Impact of disinfectants on virus function and structural integrity. *Environ. Sci. Technol.* 46 (21), 12069–12078. doi:10.1021/es3029473

Williams, O. W., Sharafkhaneh, A., Kim, V., Dickey, B. F., and Evans, C. M. (2006). Airway mucus from production to secretion. *Am. J. Respir. Cell. Mol. Biol.* 34, 527–536. doi:10.1165/rcmb.2005-0436sf

Znamenskaya, Y., Sotres, J., Engblom, J., Arnebrant, T., and Kocherbitov, V. (2012). Effect of hydration on the structural and thermodynamic properties of pig gastric and bovine submaxillary mucins. *J. Phys. Chem.* 116 (16), 5047–5055. doi:10.1021/jp212495t